Oxide muonics: II. Modelling the electrical activity of hydrogen in wide-gap and high-permittivity dielectrics

2006 J. Phys.: Condens. Matter 18 1079

(http://iopscience.iop.org/0953-8984/18/3/022)

INSTITUTE OF PHYSICS PUBLISHING JOURNAL OF PHYSICS: CONDENSED MATTER

J. Phys.: Condens. Matter **18** (2006) 1079–1119 doi:10.1088/0953-8984/18/3/022

Oxide muonics: II. Modelling the electrical activity of hydrogen in wide-gap and high-permittivity dielectrics

S F J Cox[1,2], J L Gavartin[2], J S Lord[1], S P Cottrell[1], J M Gil[3], H V Alberto[3], J Piroto Duarte[3], R C Vilão[3], N Ayres de Campos[3], D J Keeble[4], E A Davis[5], M Charlton[6] and D P van der Werf[6]

[1] ISIS Facility, Rutherford Appleton Laboratory, Chilton OX11 0QX, UK
[2] Condensed Matter and Materials Physics, University College London, WC1E 6BT, UK
[3] Physics Department, University of Coimbra, P-3004-516 Coimbra, Portugal
[4] Electronic Engineering and Physics Division, University of Dundee, DD1 4HN, UK
[5] Department of Materials Science and Metallurgy, University of Cambridge, CB2 3QZ, UK
[6] Department of Physics, University of Wales Swansea, Singleton Park, Swansea SA2 8PP, UK

Received 22 July 2005, in final form 7 December 2005
Published 6 January 2006
Online at stacks.iop.org/JPhysCM/18/1079

Abstract

Following the prediction and confirmation that interstitial hydrogen forms shallow donors in zinc oxide, inducing electronic conductivity, the question arises as to whether it could do so in other oxides, not least in those under consideration as thin-film insulators or high-permittivity gate dielectrics. We have screened a wide selection of binary oxides for this behaviour, therefore, using muonium as an accessible experimental model for hydrogen. New examples of the shallow-donor states that are required for n-type doping are inferred from hyperfine broadening or splitting of the muon spin rotation spectra. Electron effective masses are estimated (for several materials where they are not previously reported) although polaronic rather than hydrogenic models appear in some cases to be appropriate. Deep states are characterized by hyperfine decoupling methods, with new examples found of the neutral interstitial atom even in materials where hydrogen is predicted to have negative-U character, as well as a highly anisotropic deep-donor state assigned to a muonium–vacancy complex. Comprehensive data on the thermal stability of the various neutral states are given, with effective ionization temperatures ranging from 10 K for the shallow to over 1000 K for the deep states, and corresponding activation energies between tens of meV and several eV. A striking feature of the systematics, rationalized in a new model, is the preponderance of shallow states in materials with band-gaps less below 5 eV, atomic states above 7 eV, and their coexistence in the intervening threshold range, 5–7 eV.

1. Introduction: the interplay of site and charge-state for hydrogen defect centres

1.1. The stability of interstitial atomic hydrogen

We seek to model the electrical activity of hydrogen impurity in a broad selection of binary oxides. We take the unusual standpoint of considering the fate of individual hydrogen atoms, as neutral interstitial defects in an otherwise perfect lattice of the host material. While this might not be useful in mineralogy or crystallography, where neutral monatomic hydrogen centres are usually considered unimportant, it does illuminate the relevant properties of hydrogen in electronic materials, especially as concerns electronic, rather than protonic, conduction. Our main aim is to examine the systematics of the deep-to-shallow instability of interstitial hydrogen, expressed in its simplest form by expression (1). The left-hand side denotes isolated hydrogen defect centres with essentially atomic character, illustrated schematically in figure 1(a). Known to ESR spectroscopy as trapped-atom states, they are located within interstitial cages of the host lattice, though diffusion from one cage to the next may well be rapid; the unpaired or paramagnetic electron occupies a 1s(H) orbital having little overlap or admixture with surrounding atoms. Examples are H in SiO_2 (Weeks and Abraham 1965, Perlson and Weil 1974) and in Li_2O (Baker *et al* 1991). The right-hand side of expression (1) represents the opposite extreme of delocalization of the unpaired electron into conduction-band states (e_c denotes an electron at the conduction-band minimum), leaving the defect centre in its positive charge state, i.e. as the interstitial proton. In otherwise undefective oxides, the interstitial proton invariably binds to oxygen to form the hydroxide ion, as in the protonation reaction (2). The combined reaction or competition is written in (3). Conversely, atomic hydrogen is commonly generated from water or hydroxide precursor by radiolysis or photolysis (γ-rays, x-rays or UV) for ESR studies; even sunshine can be sufficient (see, for instance, Scholz and Stösser 2002)[7].

$$H^0 \text{ versus } H^+ + e_c \tag{1}$$

$$H^+ + O^{2-} \rightarrow OH^- \tag{2}$$

$$H^0 + O^{2-} \leftrightarrow OH^- + e_c. \tag{3}$$

There is a considerable distinction between reactions (2) and (3): O^{2-} ions have a strong affinity for protons but no such intrinsic affinity for neutral atomic hydrogen. In effect, the proton lowers its energy by burying into the electron cloud of the oxygen anion, which neutral hydrogen has no tendency to do, the OH antibonding level lying too high in energy. Although stabilization of the proton in this manner (2) contributes substantially to the energy balance required to drive the forward reaction (3), it is by no means always sufficient. As examples of the contrasting behaviours, hydrogen remains stable as the interstitial atom in quartz[8] but is oxidized to the proton in ZnO. If the electron is to be removed, it must be picked off by the cations. This will normally transfer the electron to the conduction-band minimum, as it does in ZnO, where the conduction band is comprised of the otherwise empty 4s(Zn) orbitals (Van de Walle 2000).

We allow that all three charge states, H^+, H^0 and H^-, can contribute to electrical activity via their interaction with carriers, whether by trapping, release or scattering. We also assume

[7] We also note two other routes to the generation of hydrogen atoms that, though not relevant to our own studies of the bulk chemicals, may contribute in actual devices. One is post-deposition hydrogenation for passivation of defects, e.g. processes such as $\equiv$Si$\cdot + H_2 \rightarrow \equiv$Si–H+H$\cdot$ for silicon dangling bonds at oxide interfaces (Stesmans and Afanas'ev 2004). Another is hydrogen release by electron impact from hydroxide ions, gate-injected electrons being able to reach considerable momentum in the ballistic régime (Yokozawa and Miyamoto 1997, Houssa 2004).

[8] In quartz, hydrogen even exhibits a hyperfine constant slightly higher than its vacuum-state value—the neighbouring closed-shell oxygen atoms of the trapping cage causing a slight compression of the 1s(H) orbital by excluding any overlap (Perlson and Weil 1974, Suryanarayana and Weil 1976).

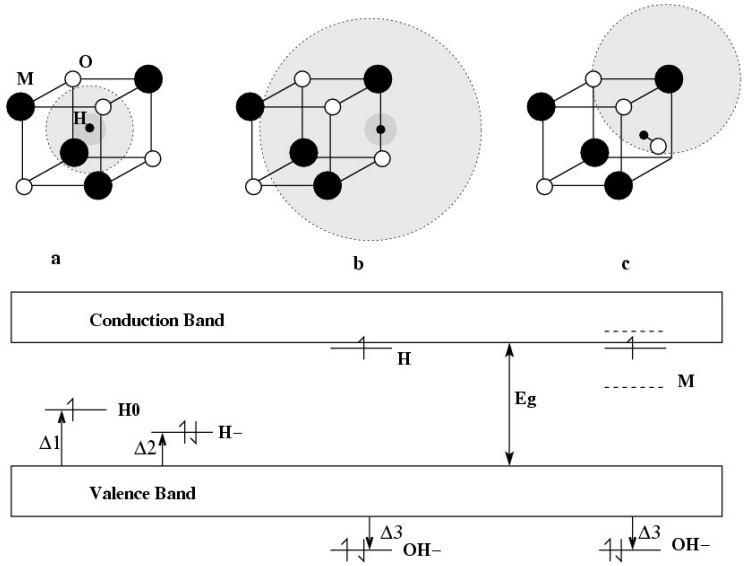

Figure 1. Schematic representations of various types of paramagnetic hydrogen centres in an oxide and their associated single particle levels: (a) a hydrogen-like deep centre with a localized, essentially atomic, wavefunction, (b) a shallow centre with a diffuse (i.e. greatly dilated) hydrogenic wavefunction centred on an OH^- molecular ion and (c) a polaronic centre near the OH^- ion—this latter has the singly occupied orbital localized on one or several metal cations (M) and may be either deep or shallow. Each carries varying degrees of distortion, small in (a) but with significant bond extension in (b) and a more severe displacement or rearrangement associated with polaron formation in (c). (The rock-salt structure is shown purely for illustrative purposes.) The labelled energy splittings are used in a rationalization of the experimental data (section 7).

that these charge states are reasonably well defined—that is, that they are integer for hydrogen in oxide dielectrics. There is no issue of variable screening by mobile electrons as there is for hydrogen in metals or metal hydrides but this is not to say that the electronic configurations are necessarily $1s^0$, $1s^1$ or $1s^2$. Most importantly, the crystallographic site varies considerably with charge state. Even in SiO_2, which is essentially covalent, the calculations of Yokozawa and Miyamoto (1997) show H^+ binding strongly to oxygen and H^- binding weakly to silicon, with significant lattice distortion in both cases. The description is confirmed and elaborated by Blöchl (2000). Interstitial H^0 does indeed have 1s character in this case: it occupies a symmetric site of low electron density: it is non-bonding and lattice relaxation is negligible. The singly occupied defect level lies deep in the gap between valence and conduction bands. However, the atomic 1s(H) character is lost completely when H^0 is complexed with an oxygen vacancy in silica, where it bridges between two Si atoms just as it does at the bond-centre site in otherwise undefective elemental silicon. The unpaired electron nonetheless remains localized on the neighbouring Si atoms in these cases (Isoya *et al* 1981, Cox and Symons 1986, Van de Walle *et al* 1989) so that the singly occupied molecular orbitals (SOMOs) again lie deep in the gap. We treat all such compact H^0 centres as belonging to the left-hand side of equations (1) and (3).

1.2. Hydrogenic (effective-mass) and polaronic shallow donors

Referring to the right-hand sides of expressions (1) or (3), the interstitial proton offers no such deep electrically active gap state. The bonding orbital for the OH^- ion typically lies below the

valence band and is doubly occupied; its antibonding orbital is invariably higher than the empty cation or conduction-band orbitals and the unpaired electron is lost to them. The interstitial proton constitutes a positively charged defect, nonetheless, so that the unpaired electron can still be weakly bound at cryogenic temperatures, creating a defect level just below the conduction-band minimum. Depicted schematically in figure 1(b), this is the classic shallow-donor state in which the singly occupied orbital is substantially, but not completely, delocalized: the charge defect is screened only at very long range. The hydrogen atom is effectively dilated by the relative permittivity (dielectric constant) of the medium and the conduction-band effective mass of the electron, so that the binding energy is reduced from one Rydberg ($R_y = 13.6$ eV) to

$$R^* \approx R_y(m^*/m_e)/\varepsilon_r^2. \tag{4}$$

In ZnO, with $m^*/m_e = 0.24$ and $\varepsilon_r = \varepsilon(\omega \to 0)/\varepsilon_0 = 8$, the expectation is $R^* \approx 0.05$ eV, defining the depth of the shallow-donor level.

The estimate of equation (4) corresponds to the effective-mass or so-called hydrogenic model[9]. We bear in mind that when transition-metal ions able to support different charge or valence states are involved, however, the electron may instead become trapped relatively close to the proton, as represented in reaction (5) and in figure 1(c). Here M is either a single cation or, more probably, a group of cations in close proximity to the proton. This is a polaronic model, giving rise to defect centres that may be either shallow or deep. The offset spin-density distribution has observable consequences for the hyperfine spectroscopy of such centres, leading to dipolar as well as contact interactions on the proton.

$$H^0 + O^{2-} + M^{(n+1)+} \leftrightarrow OH^- + M^{n+}. \tag{5}$$

1.3. Charge disproportionation and the pinning level

Processes (6)–(8) invoke electron-transfer reactions. Particularly important is the self-compensating function of charge disproportionation (6). This occurs if the Hubbard or Anderson (1975) parameter U is negative, in which case reaction (6) is exothermic. Thus whereas a truly isolated interstitial atom may be metastable against reactions (1) or (3), electron transfer can occur—whether via the conduction band or direct tunnelling—when several atoms are in communication. No electrons are released for conduction or doping in that case, unless all the relevant energy levels happen to be resonant with the conduction band. Charge transfer to or trapping at other defects, notably vacancies, can likewise suppress conduction: reactions (7) and (8) are both predicted to be exothermic in HfO_2, for instance (Gavartin 2005).

$$2H^0 \to H^+ + H^- - U \tag{6}$$

$$H^0 + V^{++} \leftrightarrow H^+ + V^+ \tag{7}$$

$$H^0 + V^+ \leftrightarrow H^- + V^{++}. \tag{8}$$

Compared with substitutional dopants or impurities, the choice of crystallographic sites available to interstitial hydrogen greatly facilitates the disproportionation reaction (6): negative U means that the Coulomb repulsion energy associated with double occupation of the defect level (the two spin-paired electrons in H^-) is more than offset by a change of site and local configuration. Neugebauer and Van de Walle (1995) anticipated that this situation should be commonplace for hydrogen in semiconductors and their argument was extended to oxide

[9] See, for instance, Stoneham (1975) and standard semiconductor texts. The term 'hydrogenic' needs to be used with some caution in the present context since, prior to the discovery in ZnO, hydrogenic shallow-donor states were unknown for hydrogen itself! The binding energy of equation (4) is not a direct indication of ionization temperature: the huge conduction-band density of states typically reduces ionization temperature to about $R^*/10k_B$, i.e. to about 50 K in the case of ZnO, so that the electron is indeed released for conduction at normal temperatures.

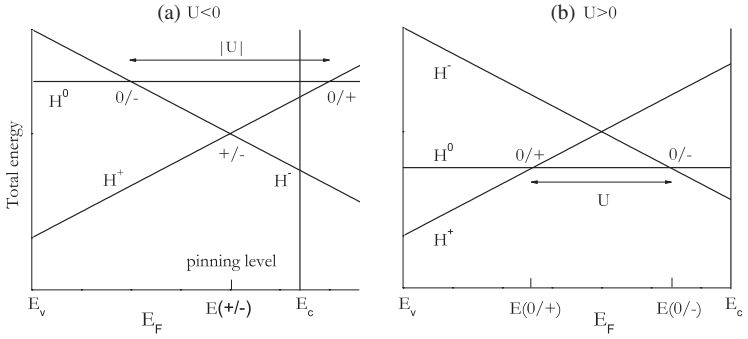

Figure 2. Formation energies of a hydrogen defect centre as a function of Fermi level E_F. The gradient with respect to E_F is equal to the charge; E_v is the top of the valence band and E_c the bottom of the conduction band. (a) is drawn for negative U, and with the $0/+$ donor level resonant with the conduction band. This leads to auto-ionization of the neutral state (shallow-donor behaviour) but the material will only be conductive under equilibrium conditions if the $+/-$ pinning level is also band-resonant; here it is shown deep in the gap. (b) is drawn for positive U, leading to the opposite ordering of $0/+$ and $0/-$ transition points, both shown deep in the gap.

dielectrics by Yokozawa and Miyamoto (1997), who found $|U|$ to be as large as several eV in silica[10]. The parameter U also corresponds to the distance between donor and acceptor levels, respectively the $(+/0)$ and $(0/-)$ switching levels, customarily illustrated as in figure 2: these diagrams are standard representations of thermodynamic switching levels for a defect having three possible charge states, adapted to the case of H^+, H^0 and H^- (see, for instance, Pantelides 1986, Neugebauer and Van de Walle 1995, Yokozawa and Miyamoto 1997, Kılıç and Zunger 2002). The implication of negative U (figure 2(a)) is that H^0 is never thermodynamically stable, in which case the observation of its ESR spectrum in quartz must be explained by the metastability of sufficiently isolated atoms. A graphic illustration of the disproportionation reaction in progress has recently been provided by molecular-dynamics simulation for two H^0 centres in HfO_2—to our knowledge the first such calculation in which the electron transfer is observed explicitly between two remote atoms (Gavartin 2005).

Negative U (driving reaction (6)) implies that the second electron in the hydrogen defect centre is bound more strongly than the first. In the hypothetical situation that monatomic hydrogen is the abundant defect, a consequence would be that the hydrogen centres then themselves define the Fermi level, pinning it halfway between their donor and acceptor levels (see, for instance, Adler and Yoffa 1976). For hydrogen, the condition corresponds to thermodynamic equilibrium between H^+ and H^- ions, so that the $H(+/-)$ transition point of figure 2(a) is referred to as the hydrogen *pinning level*. A given material will remain insulating at normal temperatures if the pinning level lies deep in the energy gap, with conduction due to other dopants suppressed, but exhibit n-type conductivity if it lies in the conduction band.

1.4. Other charge-transfer processes

Reaction (6) provides a route for generating hydride ions even in the absence of other defects or impurities. Nonetheless, the disproportionation of hydrogen is otherwise virtually unknown in chemistry, to the extent that the importance—or even the existence—of hydride ions in

[10] Negative-U behaviour is likewise calculated for hydrogen in silicon, where the hydride ion occupies a cage-centre site but the proton a bond centre (Van de Walle *et al* 1989). This contrasts with the case of H in diamond, however, which is calculated to be a strongly positive-U system, albeit with neither the neutral centre nor the negative ion having any 1s character at all (Goss 2003).

oxides is a question of some topical interest, not to say contention (see, for example, Poulsen 2001, Steinsvik *et al* 2001, Norby *et al* 2004)[11]. For the more intuitive case of positive U (figure 2(b)), the charge state which hydrogen adopts depends on the Fermi level as defined by other dopants or redox-active impurities. In principle, each of the three charge states may then be stabilized in turn by appropriate tuning of the Fermi level, a low value emptying the defect level and favouring H^+, an intermediate value (undoped material) giving H^0 and a sufficiently high value (corresponding to highly reducing conditions) encouraging double occupation to stabilize H^-. Whether U is positive or negative, isolated deep-level hydrogen centres may be seen to offer traps to either positive and negative carriers, according to the Fermi level; it acts as a compensating defect, opposing the prevailing conductivity by trapping electrons in n-type materials and releasing them in p-type. Second electron capture is represented in reaction (9) and the alternative acceptor function, namely hole-ionization, in (10). Possible generation of hydride ions by oxidation of a group of cations is represented in (11).

$$H^0 + e \leftrightarrow H^- \tag{9}$$

$$H^0 \leftrightarrow H^- + h_v \tag{10}$$

$$H^0 + M^{n+} \leftrightarrow H^- + M^{(n+1)+}. \tag{11}$$

All these redox processes are to be distinguished from the more commonly considered acid–base reactions governing the incorporation of water in defective oxides (see for example, Catlow *et al* 1995), namely the dissociation reaction (12), with ionic products stabilized as in (13). These can liberate protons for protonic conduction but cannot lead either to electronic conduction or the generation of hydride ions.

$$H_2O \rightarrow H^+ + OH^- \tag{12}$$

$$H_2O + V_O + O^{2-} \rightarrow 2OH_O^-. \tag{13}$$

In equation (13), V_O is a vacancy on an oxygen site, itself usually generated to compensate a cation charge defect. We do not use the Kroeger–Vink defect notation for fear of confusion between $OH^\bullet$ as the hydroxide ion trapped in an oxygen vacancy (where the dot indicates a positive charge defect) and as the hydroxyl radical (where it indicates the unpaired electron spin of the neutral paramagnetic species, as in the literature of ESR spectroscopy and radical chemistry, and in equation (14)). It is interesting to consider the possible importance of the hydroxyl radical, which may well be formed under radiolytic, if not under equilibrium conditions. The forward reaction (14) summarizes a route to its generation by irradiation which, like the generation of atomic hydrogen, has been used for the purposes of ESR studies, though not (to our knowledge) in oxide hosts. Even though our own measurements are made under radiolytic conditions, there is no evidence from our data that the $OH^\bullet$ radical plays any rôle. We note simply that the inverse reaction suggests a powerful acceptor function.

$$OH^- \leftrightarrow OH^\bullet + e. \tag{14}$$

1.5. Context and scope of the article

Whereas protonic conduction depends on a favourable combination of H^+ ions (usually from dissociated water) with other defects or impurities, the criteria for hydrogen-induced electronic conductivity appear to relate solely to how the energy levels for monatomic or isolated hydrogen centres are positioned relative to the conduction band edge, in otherwise

[11] We exclude from this discussion the approximately stoichiometric oxide–hydrides such as LaHO or the newly synthesized oxide–hydride perovskites: see for example Poeppelmeier (2002); we are concerned only with hydrogen as a trace impurity in binary oxides. The absence of hydrogen disproportionation in solution chemistry might be due to electron solvation, if this latter is more favourable than electron transfer via reaction (6).

pristine and undefective host material. Computational modelling by Van de Walle (2000) drew attention to this for the case of ZnO, finding that the positive ion, i.e. the interstitial proton, is the thermodynamically stable charge-state in this material. By implication, neutral atomic hydrogen donates its electron to the conduction band, as in (3), making it available as a charge carrier at normal temperatures or binding it weakly as neutral shallow donor at cryogenic temperatures. Experimental confirmation came from μSR detection of the muonium counterpart of such a state (Cox *et al* 2001a, Shimomura *et al* 2002), as well as ESR and ENDOR detection for hydrogen itself (Hofmann *et al* 2002)[12]. So far, only in ZnO has a shallow-donor hydrogen state been identified by conventional magnetic resonance, although previously unexplained features associated with hydrogen in the ESR spectra of rutile-TiO_2 deserve further investigation in this light (Chester 1961, 2004).

Considering the possibility that hydrogen might act similarly as an adventitious dopant in other oxides, the present paper (II) is devoted mainly to binary oxides that are visually transparent, i.e. to those with a band-gap above the blue-to-ultraviolet boundary at 2.5 eV. Several of these are candidate materials in the search for new thin-film insulators or high-permittivity gate dielectrics, so the issue is of some importance here: see, for instance, Robertson (2000), Shluger *et al* (2003), Houssa (2004), Stoneham *et al* (2005). Additionally, results for some semiconducting oxides—somewhat arbitrarily defined as having band-gaps corresponding to infrared or visible light—are given in an accompanying paper (Cox *et al* 2006, referred to below as Paper I). This new survey is undertaken within the framework of current predictions (summarized in section 2), again using μSR spectroscopy (introduced in section 3).

2. Theoretical predictions

Equation (3) is exemplified by calculations for H in WO_3 due to Hjelm *et al* (1996). These authors find hydrogen atoms positioned symmetrically in the interstitial cage to be unstable: the preferred configuration has the proton moved to an asymmetric hydroxide site and the electron lost to the bottom of the conduction band. From this result alone, however, it is uncertain whether the electron would remain available for conduction. Although band-resonance of the single-particle eigenvalue is a necessary condition for n-type doping, it is not sufficient, since trapping of the electron by a second hydrogen atom (reaction (6)) would suppress the conduction unless the H(+/−) pinning level is also resonant with the conduction band. The calculations of Van de Walle (2000) find this to be the case for ZnO, confirming hydrogen as a dopant in this, a material that is on the verge of important device applications—considered for instance as a challenge to GaN in optoelectronics. The systematics of hydrogen-induced electronic conductivity amongst a wider selection of oxides are discussed in these terms by Kılıç and Zunger (2002), whose paper prompted the present experimental survey. Their calculations find an apparently common value for the H(+/−) pinning level in MgO, ZnO, CdO and SnO_2 (figure 3(a)), near −3 eV on the vacuum scale, and they assert that it will be the same for other binary oxides. The majority of the other oxides considered by these authors appear to be those that figure in the band-offset diagrams compiled from electrochemical data, e.g. by Butler and Ginley (1978) and Schmickler and Schultze (1986). One of these diagrams is redrawn in figure 3(b), where we have limited the selection mainly to non-magnetic oxides in anticipation of our own experimental method and superimposed the

[12] μSR = muon spin rotation, relaxation and resonance (see for example Brewer *et al* 1975), the acronym contrived to resemble ESR = electron spin resonance. ENDOR = electron nuclear double resonance, to which μSR spectra such as that of figure 4(a) are somewhat analogous.

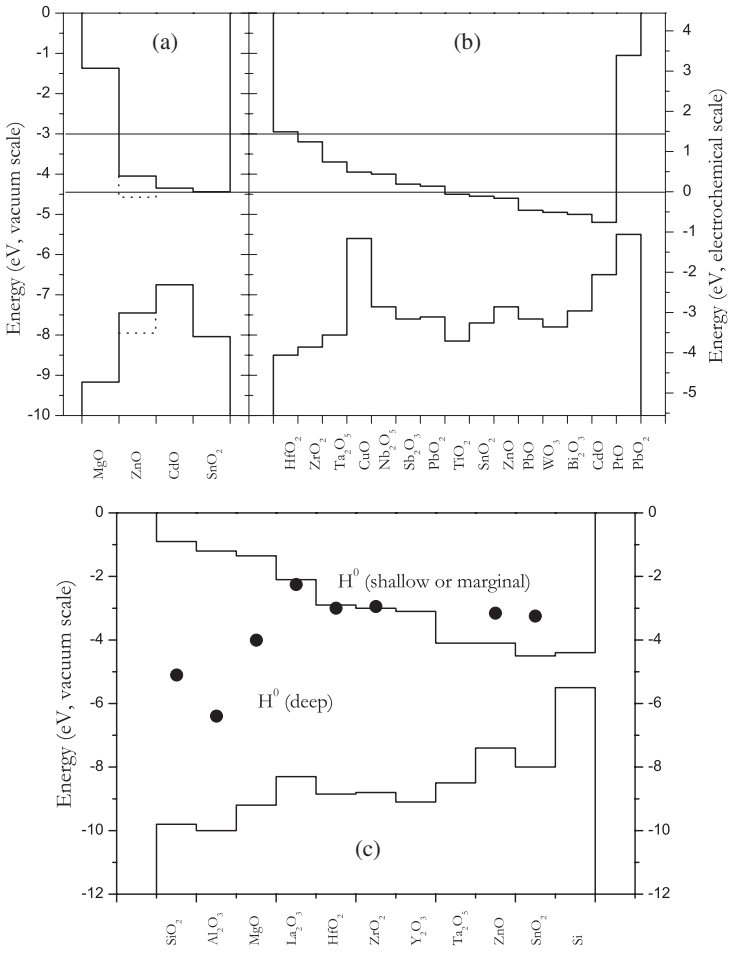

Figure 3. Band offset diagrams, adapted from those due to (a) Kılıç and Zunger (2002), (b) Schmickler and Schultze (1986) and (c) Robertson (2000). The lower histogram represents the valence-band maxima and the upper the conduction-band minima. Superimposed in (a) and (b) are the H(+/−) pinning levels of Kılıç and Zunger (2002) (upper line) and of Van de Walle and Neugebauer (2003) (lower line; the dotted amendments represent their band-edge positions for ZnO). In the pinning-level model, n-type conductivity is induced when this level lies in the conduction band but not when it lies deep in the gap. In (c), the approximate offsets are shown relative to silicon (at right) and H^0 energy eigenvalues added from Peacock and Robertson (2003).

putative pinning level:[13] the implication is that hydrogen should cause n-type conduction in all materials whose conduction-band minima fall below this line. In figure 3(a), therefore, the prediction of hydrogen-induced conductivity in ZnO, CdO and SnO_2 is the direct result of computational modelling; for the materials in 3(b), however, it relies on the validity of a common pinning level and the accuracy of the electrochemical data.

[13] CuO is retained for the comparison with Cu_2O, discussed in Paper I, although Madelung (1996) gives the optical gap for CuO as zero in the visible and near infrared. CdO appears to be represented with its direct gap; we treat it as a semiconducting oxide in Paper I, the indirect gap being less than 1 eV. Otherwise, similar predictions are obtained using the pinning level on band-offset diagrams due to Memming (1983). A labelling error in figure 26 of Cox (2003a) is corrected. The conduction-band minimum of PbO_2 is not given by Schmickler and Schultze; we have constructed it at the right of figure 2(b) by adding the experimental bandgap to their valence-band maximum.

The identical concept of a universal pinning level for hydrogen is expressed by Van de Walle and Neugebauer (2003), supported by calculations for a different selection of binary semiconductors, with oxides represented by the contrasting cases of ZnO and SiO_2. Most of their calculations are for tetrahedrally coordinated materials, however, and their supporting arguments imply covalency. With oxygen coordination commonly varying between 2 and 8, it is of interest to test their predictions on materials of different structure and ionicity. Their universal level lies somewhat lower than that of Kılıç and Zunger (2002), namely at −4.5 eV on the vacuum scale[14], implying that fewer materials in figure 3(b) are at risk from hydrogen-induced conductivity.

Robertson (2000) focusses on a selection of oxides that are candidate high-permittivity dielectrics and calculates their band offsets relative to elemental silicon, this being a major consideration in the utility of gate oxides in real devices. Low electron affinity of the gate oxide may be seen to have a double benefit. It guarantees a good conduction-band offset with respect to silicon, reducing leakage current due to electron tunnelling through nano-scale oxide layers; it also lowers the risk of hydrogen-induced conductivity in the oxide layer, according to the pinning-level model. Peacock and Robertson (2003) do not invoke this model but calculate instead the single-particle eigenvalues or energies of H^0 defects, noting that these lie deep in the gap for interstitial atomic states but that shallow-donor behaviour results when they move up into the conduction band. They do not find any universal threshold or alignment but separately predict hydrogen to be shallow in ZnO, HfO_2, ZrO_2, SnO_2 and La_2O_3 as well as (Robertson 2004) in TiO_2 and Y_2O_3.[15] Shown in figure 3(c), their results reveal another issue, namely that electrons released via process (3) will not remain in a thin oxide layer (except perhaps in SnO_2) but will sink to the adjoining silicon: the problem of hydrogen-induced conductivity is then exchanged for one of fixed positive charge at the interface. When H^- is the stable charge state in the oxide, as in Al_2O_3 (and also in Y_2O_3, according to Ragnarsson *et al* 2001), the fixed charge is negative.

Since HfO_2 and ZrO_2 appear currently to dominate the search for new gate dielectrics, the question is particularly important here. Shluger *et al* (2003) find the issue of whether H^0 or H^+ is the more stable in these two materials to be marginal, and so have performed calculations for each of the several crystallographic structures that they can adopt. They conclude that H^+ is the stable state in both monoclinic and tetragonal ZrO_2, as well as in monoclinic HfO_2, but that H^0 may be stabilized by the larger gap in tetragonal HfO_2. Even then, H^0 is only metastable as the isolated atom, communication between a pair of H^0 atoms leading to disproportionation as in reaction (6).

Rather few values of U are given in the literature. Gavartin *et al* (2005) calculate a particularly high value (−2.7 eV) in HfO_2—somewhat larger than the −1.6 eV of Kang *et al* (2004), though with a similar pinning level in the gap. These authors also find hydrogen to constitute a shallow donor when complexed with an oxygen vacancy in monoclinic hafnia. Recalling the value of −2.4 eV calculated for H in SiO_2 by Yokozawa and Miyamoto (1997) we note that their expectation that U will increase in magnitude with the ionicity or polarity of the material does not appear to be borne out, Kılıç and Zunger (2002) finding several values close to zero. To date, no experimental values of U for hydrogen in oxides have been reported.

[14] The pinning level of Van de Walle and Neugebauer (2003) thus lies close to the origin of the electrochemical energy scale, as these authors justify with charge-neutrality and chemical arguments. This is the standard hydrogen-electrode potential defined by the reaction $H_2 + 2H_2O \leftrightarrow 2H_3O^+ + 2e$, which may be compared and contrasted with equation (3), both being in part driven by stabilization of the proton. Note, however, that the H_2 dissociation energy does not figure in the energy balance for (3); this latter is about 4.8 eV *in vacuo*, though generally reduced in condensed phases.

[15] Peacock and Robertson (2003) also give predictions for ternary oxides of the perovskite family; we do not consider these here but they are the subject of a separate μSR study by one of us (Keeble 2006).

3. Oxide muonics

Given the difficulty of translating purely electrical measurements into atomistic pictures of hydrogen behaviour, we have begun a systematic survey for other oxides using positive muons in place of protons and muonium as a pseudo-isotope of hydrogen. We introduce the term *muonics* to describe the relevant properties of muonium, notably as an experimentally accessible model for the electronic structure and electrical activity of hydrogen. The experiments exploit all three variants of μSR spectroscopy (muon spin rotation, relaxation and resonance), as summarized in Paper I: this is in essence a combination of ion implantation and a highly sensitive form of magnetic resonance, accessing all three muonium charge-states as well as the interplay between them on capture and loss of charge carriers.

Thanks to the various advantages of μSR spectroscopy for this purpose, details of local electronic structure are known in rather more materials for muonium than for paramagnetic hydrogen. This is certainly true amongst semiconductors, with both deep and shallow muonium states known within the II–VI and III–V compounds (Patterson 1988, Gil *et al* 2001a, Davis *et al* 2003). In these two families, the data are generally supportive of threshold models of the deep-to-shallow transition, with a critical electron affinity near 3.5 eV: muonium hyperfine constants in these materials show increasing dilation of the quasi-atomic states as the threshold is approached, followed by a remarkably sharp or critical transition to the shallow or extended states (Cox 2003a). It happens that the majority of materials previously studied in this way have tetrahedral coordination, so the importance of testing threshold or alignment models on other structures—amongst oxides especially those with differing oxygen coordination—is underlined.

Validation of the muonics principle requires a critical comparison of H and Mu centres in materials where both are known. Not so many examples exist amongst oxides, so it is fortunate that they include the contrasting cases of SiO_2 and ZnO. In quartz, hydrogen and muonium both exhibit trapped-atom states, with hyperfine constants close to, but not identical with, the respective free-atom values (Weeks and Abraham 1965, Myasischeva *et al* 1967, 1968, Minaichev *et al* 1970a, 1970b, Brewer *et al* 1973, Weil 1981). In frequency units, the free-atom hyperfine constants are 1.42 GHz for H and 4.46 GHz for Mu: these values are related by the ratio (3.18) of the muon and proton magnetic moments, with a small correction for electron reduced masses. That is, the spin densities on proton and muon are the same to within a few per cent—a difference that can be traced to the greater zero-point energy of muonium in the interstitial cage. The same is true of alkali halides, where a more extensive comparison is possible. For these materials, H is known to ESR in every member of the family; there is greater deviation of the hyperfine constants from the free-atom value and the variation is exactly mimicked in muonium spectroscopy (Spaeth 1986, Baumeler *et al* 1986, Kiefl *et al* 1986). In semiconductors, notably silicon, where states of greater delocalization are found, the similarity extends from the hyperfine spectroscopy (reflecting details of electronic structure) to the actual positions of deep donor and acceptor levels in the energy gap (Lichti 1995, Bonde Nielson *et al* 1999). Although the muon is considerably lighter than the proton, $m_p/m_\mu \approx 1/9$, the point here is that parameters such as donor depths refer to *differences* in configurational energies, so that zero-point energy corrections are small and calculable (Cox 2003a). Analogous shallow-donor states of hydrogen and muonium are found in ZnO, so that the muonium–hydrogen analogy may be taken to extend across the deep-to-shallow transition.

Interstitial atomic muonium was known in the early μSR literature as *normal muonium*. This designation distinguishes the isotropic muonium states in SiO_2 and Si, for instance, from the highly anisotropic *anomalous muonium* which was found to coexist in Si (Brewer *et al* 1973). This latter is now known to be a deep-donor state at a bond-centre site in Si and we show

below that there may be similar states in HgO and GeO_2. Amongst the oxides, normal muonium was most studied in SiO_2 but was also known in BeO, CaO and MgO (Brewer 1981, 1983, Spencer *et al* 1984, Kiefl *et al* 1986). It has also been studied extensively in H_2O, both ice and water (see, e.g., Percival *et al* 1985). The room-temperature yields per implanted muon, from these studies and our own, are included in table 2. Muonium in Al_2O_3 could only be inferred somewhat indirectly, posing a long-standing puzzle about its precise formation mechanism—lately with the added contention that this may involve an interplay with the negative ion, i.e. the hydride-ion analogue (Minaichev *et al* 1970a, 1970b, Kreitzman *et al* 1986, Storchak *et al* 1997, Brewer *et al* 2000). Observation of muonium in fine oxide powders (Al_2O_3, MgO and SiO_2) raises quite different issues of surface mechanisms that are also still unresolved (Kiefl *et al* 1982, Harshman 1986, Donnelly *et al* 2006). In the ESR literature, atomic hydrogen is reported in quartz (Weeks and Abraham 1965, Perlson and Weil 1974), Li_2O (Baker *et al* 1991), as well as in ice and water (Roduner *et al* 1995) but otherwise, surprisingly, only in more complex oxides (Gross *et al* 2001, Scholz and Stösser 2002).

Of the many variants of the μSR technique, we chiefly make use of two in the present study. For the shallow-donor search we use muon spin rotation, i.e. the precession of the muon spin in a transverse magnetic field, looking for broadening or splitting of the spectrum characteristic of weak hyperfine interactions. This is introduced in section 3.1 and exploited in section 4. For the trapped-atom states with much higher hyperfine parameters we use instead a decoupling technique in longitudinal field, introduced in section 5 and exploited for other deep states in section 6.

3.1. The shallow-donor muonium state in ZnO—a reappraisal

The deep and shallow states contrast both in their hyperfine spectroscopy and in their ionization behaviour. Thus normal muonium in SiO_2 has a hyperfine constant of 4.5 GHz, close to the vacuum-state value, and its signal persists in μSR spectra to over 1000 K. Hydrogen atoms trapped in suitably symmetric cage-like structures in more complex oxides are likewise detectable by ESR spectroscopy to well above room temperature (Scholz and Stösser 2002). In ZnO, on the other hand, the muonium electron is so weakly bound that the hyperfine constant is only 0.5 MHz, i.e. smaller by four powers of ten. One can say that the orbital is spread out as a packet of conduction-band states: this character is confirmed by double-resonance measurements of the electron g-factor, in ZnO as in CdS and CdSe (Lord *et al* 2004). The paramagnetic signal in ZnO drops in intensity gradually above 10 K, more steeply above about 30 K, and is lost altogether by 50 K.

Both the spectroscopy and ionization behaviour of muonium in ZnO are reproduced in figure 4, illustrating the principle of our search for similar shallow-donor states in other oxides. The μSR spectrum is the frequency transform of the muon spin rotation signal in a weak transverse field—here 20 mT. The central line at 2.72 MHz corresponds to muon Larmor precession in this field ($\gamma_\mu/2\pi = 0.136$ MHz mT^{-1}) and so is assigned to the Mu^+ fraction. By analogy with the protonation reaction (2), which the calculations of Van de Walle (2000) confirm will occur in ZnO, the interstitial muon is assumed to be stabilized by incorporation into a closed-shell molecular species resembling the hydroxide ion:

$$\mu^+ + O^{2-} \rightarrow OMu^-. \tag{15}$$

The two satellite lines with their characteristic hyperfine splitting reveal the paramagnetic Mu^0 fraction; their distinctive powder-pattern lineshape indicates a degree of anisotropy in the hyperfine tensor, so that there are dipolar as well as contact terms. Whereas for substitutional donors such as P in Si, the spin-density distribution has close to spherical symmetry, centred

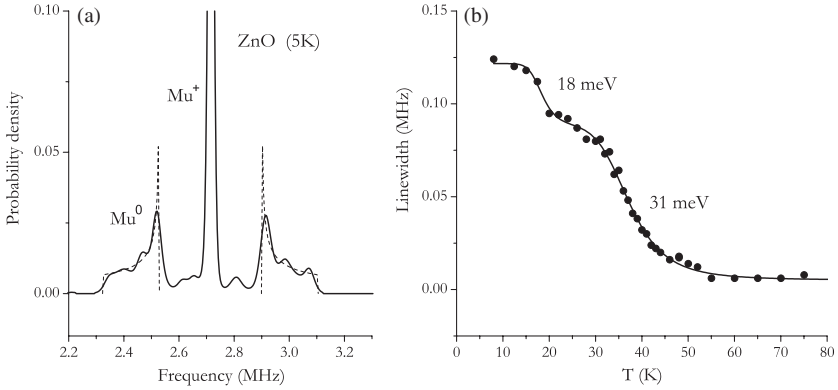

Figure 4. μSR spectrum for shallow-donor muonium in ZnO and the variation with temperature of its overall linewidth (b). The maximum-entropy spectrum is reproduced from Cox *et al* (2001a); the superimposed dashed line is a model powder-pattern lineshape. The data set in (b) is the same as used by Gil *et al* (2001a), reanalysed as described in the text.

on the charge defect, it seems likely that this cannot be so for interstitial H or Mu in oxides. In particular, there can be essentially no α-spin density on the proton or muon itself, since this would imply occupation of the hydroxide antibonding orbital, which lies prohibitively high in energy. (It is not depicted in figures 1(b), (c), since it invariably lies above the conduction band: see, for example, Peacock and Robertson (2003) or Kang *et al* (2004).) By implication, the isotropic component of the muon hyperfine constant, i.e. the contact term, is probably not positive but negative, representing spin polarization of the bonding and valence electrons[16]. For the transition-metal oxides, the apparently large dipolar terms are consistent with a polaronic rather than hydrogenic model, as illustrated in figure 1(c).

When easily resolved, the amplitudes of the central line and satellites provide a measure of Mu^+ and Mu^0 fractions and it is their variation with temperature in an equilibrium model that has hitherto been analysed for ionization energy or donor depth (Gil *et al* 2001a, Cox *et al* 2001a, Shimomura *et al* 2002). In fact, it is not obvious whether a dynamic or thermal equilibrium between Mu^0 and Mu^+ can be assumed if the satellites remain visible. Too fast an exchange would broaden and collapse them towards the central line—and indeed they commonly appear merged or unresolved in many of our other oxide spectra, as we report below. Recent simulations of the similar effect of spin-exchange on shallow-donor spectra show that the satellites are lost when the spin-exchange rate exceeds about 4 times the hyperfine constant (Senba 2005). For the ZnO case this would occur for as few as 4 or 5 exchange events within the muon lifetime.

Exactly how the variations of the paramagnetic (Mu^0) and diamagnetic (Mu^+) fractions with temperature should be analysed to extract the donor depth thus remains uncertain. Thermodynamic equilibrium cannot be assumed for muon implantation. We use a pulsed beam, introducing about 10 energetic muons per cubic mm of sample at any one time: at this dilution they cannot disturb any pre-existing Fermi level globally, although they undoubtedly do so locally or momentarily. This is one important difference with the case which we wish to model, namely that of hydrogen as an abundant impurity, itself controlling or modifying

[16] Previous arguments relating the contact term to the hydrogenic radius (Cox 2003a, Cox *et al* 2001a, Gil *et al* 2001a) may therefore, for the oxides at least, be invalidated.

the steady-state carrier density[17]. An important question is whether the electron is first captured irrespective of temperature and then lost through ionization in this temperature range or whether the probability of capture—or of cascade from an excited state—is itself temperature dependent. The matter is discussed critically by Storchak *et al* (2004) but is still not fully resolved. For several materials we have confirmed (by means of radio-frequency resonance or final-state analysis) that there is no measurable delay to formation of the shallow state, so in the following we adopt the ionization model. If there is a cascade of the electron down to the ground state, the bottleneck energies are in any case of the same order as the donor depth. In the following, the ionized (f) and unionized ($1-f$) muonium fractions are related by the purely empirical expression $f/(1-f) = N\exp(-E_\mathrm{i}/kT)$. That is, the separate fractions are

$$f = N\exp(-E_\mathrm{i}/kT)/(1+N\exp(-E_\mathrm{i}/kT)) \tag{16}$$

and

$$1-f = 1/(1+N\exp(-E_\mathrm{i}/kT)). \tag{17}$$

Here the activation energy E_i is taken to be an effective ionization or binding energy for the muonium electron and is the principal parameter to be extracted from the data. We make no use of the density-of-states parameter N, although this also affects the width of the ionization régime and varies considerably from one material to another.

Anticipating cases where the satellites are poorly resolved, we apply a method of analysis where the spectrum is approximated by a single Lorentzian, focussing attention on the temperature dependence of overall linewidth λ. The analysis is performed in the time domain: that is, the precession signal is fitted to a single oscillatory function $\mathrm{e}^{-\lambda t}\cos(\omega_\mu t)$, centred on the muon Larmor frequency and with exponential damping imposed. This method is tested using ZnO data in figure 4(b). The temperature dependence of λ shows two steps of the form (17), for which the fitted activation or ionization energies are $E_\mathrm{i} = 18$ and 31 meV. It is the larger value that we attribute to muonium ionization; interpreted as a carrier activation energy in thermal equilibrium, it equates to the donor depth if compensating acceptors are present but to one-half the donor depth for the case of no compensation. In round numbers, that is, the muonium donor depth must lie between 30 and 60 meV, this method of analysis closely reproducing previous results (Gil *et al* 2001a, Davis 2004). The donor depth for hydrogen itself in ZnO was similarly found to lie between 35 and 66 meV, according to the analysis model (Hofmann *et al* 2002).

We tentatively attribute the weaker variation (18 meV) in our μSR data below 20 K to communication with native donors via hopping conduction, following the interpretation of a similar effect in CdTe (Corregidor *et al* 2004). Again, there is some similarity with the ESR data for ZnO:H, where the low-T variation is weaker still (4 meV), but extends almost to 40 K. It is likewise attributed to potential fluctuations (Hofmann *et al* 2002). Alternatively, these low-T effects may represent an artefact of spin–lattice relaxation: the Orbach process found for shallow-donor phosphorus centres in silicon gives a very similar activation energy (123 K, equivalent to 11 meV) as well as relaxation times in the appropriate microsecond range (Tyryshkin *et al* 2003, plus references therein). In the latter case, the Orbach energy represents a splitting of the donor level, i.e. some fraction of the full donor depth.

[17] In the case that a high concentration of other donors is present, our activation energies may even refer to the differential donor depth, but this is unlikely in our nominally undoped samples.

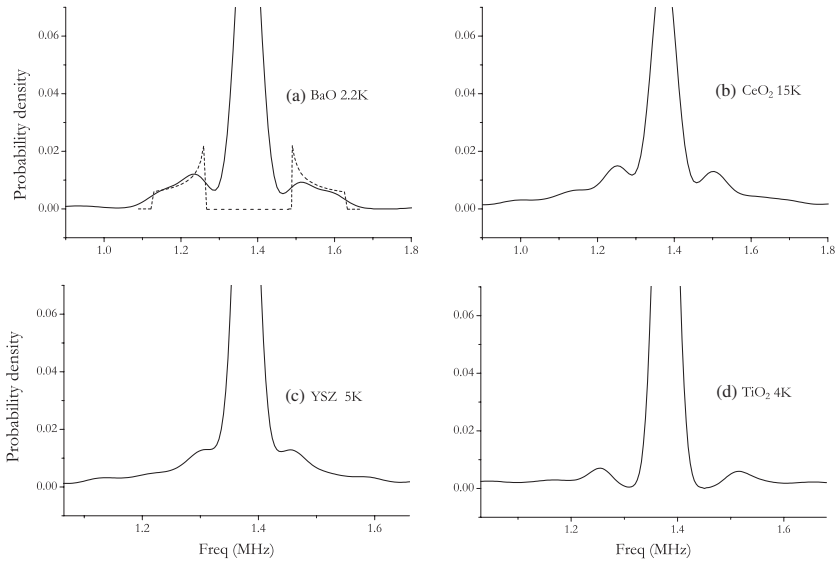

Figure 5. Muon spin rotation spectra for four oxides with weak nuclear magnetism, showing hyperfine satellites suggestive of shallow-donor muonium states. An internal correlation (smoothing) of 50 kHz has been imposed in the maximum-entropy transforms to suppress ringing artefacts. The spectrum for BaO resembles the (unsmoothed) simulated powder-pattern lineshape, superimposed as the dashed line in (a).

We turn now to the new data on the other oxides, obtained at ISIS using a combination of the MuSR, EMU and DEVA instruments[18]. A summary account for a few of the materials has been given in (summer 2004) conference proceedings (Cox *et al* 2005).

4. The shallow-donor search

4.1. Materials with weak or sparse nuclear moments

Of the various materials in which shallow-donor hydrogen states have been predicted, we begin our search in those which have the weakest nuclear magnetism, so that small muonium hyperfine splittings would not be obscured by dipolar broadening. Referring to table 1, where the relevant nuclear parameters are listed, we present in this section new data on oxides of Ba, Ce, Hf, Pb, Sn, Ti, W, Y and Zr.[19] Titania was studied in both its rutile and anatase forms and zirconia in both its monoclinic and cubic polymorphs, this latter stabilized with 9.5% yttria.

[18] WWW.ISIS.RL.AC.UK/MUONS. We do not expect to be able to detect or characterize Mu^0 centres in magnetic materials, where paramagnetic muonium is usually subject to strong depolarization. The particular case of CuO is included in figure 2(b) since it is mentioned briefly in Paper I. When interest focusses not on the chemical fate of the muon, on the other hand, but on the response of its spin to the magnetic structure, dynamics and phase transitions of the host material, μSR studies have in many instances proved immensely valuable or provided unique data. These important applications of muon spin rotation and relaxation in magnetic materials are reviewed, for instance, by Dalmas de Réotier and Yaouanc (1997), Amato (1997). In oxides it is usually the O^{2-} ions which mediate the superexchange between magnetic cations; however, recent use of μSR spectroscopy in establishing the highly polarizable hydride ion as a significant exchange path in oxide–hydrides is noteworthy in this context: see Blundell *et al* (2003).

[19] GeO_2 proves to be an unusual case and is covered in section 5 below, together with new data on SiO_2. Ag_2O and CdO figure in Paper I, CdO showing resolved shallow-donor hyperfine splittings.

Figure 5 shows examples of the spectra. Hyperfine satellites are quite clearly seen in BaO (a) where, as for ZnO in figure 4, the characteristic Pake-doublet or powder-pattern lineshape is evident. The spectrum for CeO_2 (b) is more typical of our other polycrystalline samples, with broader wings suggestive either of greater anisotropy in the hyperfine tensor or the onset of some spin dynamics. (Note that Ce is one of only two elements to have no naturally occurring dipolar nuclei.) Similar spectra are seen for Y_2O_3 and La_2O_3. For yttria-stabilized cubic zirconia (YSZ or c-ZrO_2) the satellites are likewise not so clearly resolved but appear more as shoulders on the central Larmor-precession line (c); their integrated intensity is 25%, as though one muon in four picks up an electron on implantation to form a weakly bound paramagnetic state. In the spectrum for single-crystal rutile-titania (d), the integrated intensity of the two satellites accounts for 20% of the total muon polarization.

Several of the other materials, while showing no clear structure in their spectra, show an otherwise unexpected increase of linewidth at cryogenic temperatures. For these, it appears that hyperfine satellites are present but are either unresolved (e.g. due to large anisotropy, in polycrystalline spectra) or are collapsed to a single broad line by short spin-state lifetimes (e.g. due to spin–lattice relaxation, spin exchange or charge exchange of the unpaired electron). Data for eleven materials are shown in figure 6: here the Lorentzian linewidth λ is synonymous with the damping rate of the muon spin rotation signal, analysed in the time-domain as a single-component function of the form $e^{-\lambda t}\cos(\omega_\mu t)$, as are the older ZnO data in figure 4(b).

One of the materials represented in figure 6 shows no signs at all of paramagnetic muonium states. This is PbO_2, for which the Larmor precession signals account for the full incoming muon polarization at all temperatures investigated (5–300 K) and for which the damping rate exhibits a plateau at low temperature, the value of 0.02 μs^{-1} representing the dipolar linewidth for static muons. The gradual decrease in linewidth, just discernible above about 100 K for PbO_2, undoubtedly represents motional narrowing due to the onset of muon diffusion[20]. Although PbO_2 figures in the Kılıç and Zunger (2002) list of materials susceptible to hydrogen doping, the prediction seems to be at variance with their own pinning model. The conduction-band minimum does not figure in the band-offset diagram due to Schmickler and Schultze (this is perhaps the origin of the confusion) but, when constructed as at the right of figure 3(b), it lies safely above the threshold. The curious feature of our μSR data, therefore, is not the lack of a shallow-donor state in PbO_2 but the absence of normal atomic muonium.

Of the other materials, the cases of WO_3 and CeO_2 are particularly striking: nuclear magnetism is quite negligible in these materials so that the increase in linewidths below 100 K can only represent some involvement of unpaired electronic spins. WO_3 is the parent compound to a variety of fascinating photochromic materials and is remarkable in that it changes colour on warming in hydrogen—a fact that was noted already in the early 19th century (Berzelius 1815, cited by Hjelm *et al* 1996). In this material, it appears that equation (3) applies not just to isolated centres but accounts for the exothermic uptake of high concentrations of hydrogen, with an effect on electrochemical and photochromic properties comparable with those induced by interstitial Na and Li. The present data make a strong case for the existence of shallow-donor muonium states and, by inference, for the possibility of hydrogen-induced conductivity.

[20] Noteworthy here are accounts of muon site preferences—all of the hydroxide type—and the onset of mobility in the early μSR literature on magnetic oxides: in Fe_2O_3, for instance, there is evidence of some form of local motion just above 100 K, fast long-range muon diffusion becoming apparent only above 500 K (Ruegg *et al* 1981, Boekema *et al* 1981). A similar transition between local and long-range proton motion is actually seen in molecular-dynamics simulations for HfO_2—the former making and breaking OH bonds within a particular interstitial cage when the O–O distance is minimum, the latter involving OH reorientation (Gavartin 2005). Given the diversity of structures, however, this behaviour could vary considerably from one oxide to another: an onset of local motion as low as 55 K is reported in CuO (Duginov *et al* 1994a).

Table 1. Nuclear parameters and linewidth contributions. The contribution to the second moment of the μSR lineshapes is given for a single cation at a fixed distance from the muon, weighted by isotopic abundance and summed for the different isotopes where appropriate (after Pratt, unpublished). It is given relative to niobium, set at 100. The final column gives actual predicted linewidths for ZrO_2 and HfO_2—two oxides for which these have been calculated for specific sites and structures (Lord, this work); the values labelled (M) are experimental μSR linewidths for the corresponding elemental metals, scaled from zero-field data where necessary (Schenck 1985, Hartmann *et al* 1992, Harris 1991, Cox and Hartmann 2006): they are given as an upper limit for nuclear broadening in the oxides. The horizontal line roughly demarcates materials with weak and strong nuclear magnetism: hyperfine splittings for shallow-donor muonium should be visible, if present, for entries 1–21, but are likely to be obscured by the nuclear broadening for entries 22–30.

		Dipolar nuclei	Natural abundance (%)	Spin	Moment	M2 contribution (relative to Nb)	Predicted linewidth (μs^{-1})
0	All	^{17}O	0.04	5/2	−2.6	0.004	
1	CaO	^{43}Ca	0.14	7/2	−1.3	0.006	
2	CeO_2	None				0	
3	WO_3	^{183}W	14	1/2	0.1	0.02	
4	IrO_2	^{191}Ir	37	3/2	0.15		
		^{193}Ir	63	3/2	0.16	0.09	
5	ZnO	^{67}Zn	4	5/2	0.88	0.10	
6	Ag_2O	^{107}Ag	52	1/2	−0.11		
		^{109}Ag	48	1/2	−0.13	0.10	0.016 (M)
7	SiO_2	^{29}Si	5	1/2	−0.55	0.10	
8	Y_2O_3	^{89}Y	100	1/2	−0.14	0.12	
9	GeO_2	^{73}Ge	8	9/2	−0.88	0.15	
10	SrO	^{87}Sr	7	9/2	−1.1	0.22	
11	MgO	^{25}Mg	10	5/2	20	0.22	
12	TiO_2	^{47}Ti	7	5/2	−0.79		
		^{49}Ti	5	7/2	−1.1	0.32	0.012–0.025 (M)
13	RuO_2	^{99}Ru	13	5/2	−0.72		
		^{101}Ru	17	5/2	−0.72	0.42	
14	HgO	^{199}Hg	17	1/2	0.51		
		^{201}Hg	13	3/2	−0.56	0.42	
15	HfO_2	^{177}Hf	19	7/2	3.5		
		^{179}Hf	14	9/2	−0.64	0.47	0.028–0.034
16	PbO, PbO_2	^{207}Pb	22	1/2	0.59	0.50	0.06 (M)
17	SnO_2	^{115}Sn	0.3	1/2	−0.92		
		^{117}Sn	8	1/2	−1.0	0.52	0.032 (M)
18	BaO	^{135}Ba	7	3/2	0.84		
		^{137}Ba	11	3/2	0.94	0.52	
19	ZrO_2	^{91}Zr	11	5/2	−1.3	0.57	0.030–0.036
20	CdO	^{111}Cd	13	1/2	−0.59		
		^{113}Cd	12	1/2	−0.62	0.59	
21	PtO, PtO_2	^{195}Pt	34	1/2	0.61	0.81	0.043 (M)

HfO_2 and ZrO_2 are two of the prime candidates for new thin-film insulators and high-permittivity gate dielectrics (see, for instance, Robertson 2000, Shluger *et al* 2003, Houssa 2004, Stoneham *et al* 2005). For these important materials we have made explicit estimates of the expected nuclear contribution to the μSR linewidths, for various candidate muon sites of the hydroxyl type: we obtain values between 0.028 and 0.034 μs^{-1} in HfO_2 and between 0.030

Table 1. (Continued.)

		Dipolar nuclei	Natural abundance (%)	Spin	Moment	M2 contribution (relative to Nb)	Predicted linewidth (μs^{-1})
22	BeO	^{9}Be	100	3/2	−1.2	5	0.14 (M)
23	Ta_2O_5	^{181}Ta	∼100	7/2	2.3	15	0.1 (M)
24	Cu_2O	^{63}Cu	69	3/2	2.2		
		^{65}Cu	31	3/2	2.4	18	0.25 (M)
25	La_2O_3	^{139}La	99.9	7/2	2.8	21	
26	Sb_2O_3, Sb_2O_5	^{121}Sb	57	5/2	3.4		
		^{123}Sb	43	7/2	2.5	27	
27	Li_2O	^{6}Li	8	1	0.82		
		^{7}Li	92	3/2	3.3	34	0.29 (M)
28	Al_2O_3	^{27}Al	100	5/2	3.6	40	
29	Bi_2O_3	^{209}Bi	100	9/2	4.1	44	0.15 (M)
30	Nb_2O_5	^{93}Nb	100	9/2	6.2	100	0.33 (M)

and 0.036 μs^{-1} in ZrO_2. The upper values are drawn as dashed lines in figures 6(c), (d)[21]. The increases beyond these values can again only be ascribed to the proximity of unpaired electrons. It seems likely that the same is true of the other materials where more or less abrupt increases of linewidth are seen, with various onset temperatures below 100 K. These are TiO_2, where the increase correlates with the appearance of satellite lines, as well as Y_2O_3 and SnO_2, for which shallow hydrogen states have explicitly been predicted.

The curves in figure 6 describe variations of linewidth of the form $1/(1 + N\exp(-E_i/kT))$, as suggested by equation (17). The simplest interpretation is that the fitted steps represent ionization of weakly bound muonium states by direct loss of the electron to the conduction band, with the ionization energies E_i giving a rough guide to the corresponding donor depths[22]. We make no attempt to fit the more gradual reduction of linewidth at higher temperatures, i.e. the motional narrowing of the nuclear contribution, where significant. The activation energies for disappearance of the paramagnetic contribution are all below 20 meV, with the corresponding ionization temperatures all below 100 K, and so appear largely appropriate to a shallow-donor model of the muonium states. This preliminary conclusion is corroborated by comparison with effective mass theory (where possible) in section 7, as well as by further analysis of the precession signals in appendix A. It is important, however, to distinguish between electronic moments centred on or near the muon, i.e. between the formation of bound muonium states and the effect of more distant pre-existing paramagnetic impurities. We discuss first the impurity question, showing that it can be discounted.

4.2. Paramagnetic impurities

Dilute paramagnetic impurities give rise to a Lorentzian field distribution throughout the lattice, which would be reflected in the μSR lineshape and contribute to its overall width. Such

[21] Our dipolar sums assumed cubic lattice structures for simplicity. It is unlikely that the polycrystalline averages would be very different in the monoclinic or tetragonal forms, or greatly altered by the local quadrupole interactions. A similar linewidth might be expected in YSZ, but for the greater availability of vacancy sites. The interpretation of experimental linewidths in ZrO_2 by Amato *et al* (2003) in terms of nuclear broadening and motional narrowing is in our view untenable, therefore: these authors report linewidths similar to our own (0.15 MHz) in natural ZrO_2, with the value rising to over 0.25 MHz below 10 K in an ultrapure sample.

[22] It is worth mentioning that the density of states term N takes its largest value in our data for rutile TiO_2—a single-crystal sample for which the hyperfine satellites are well resolved. A much smaller value in fine-powder anatase is in large part responsible for the wider ionization range. In an equilibrium model, N counts conduction-band states in the volume around the muonium centre which is free of other defects.

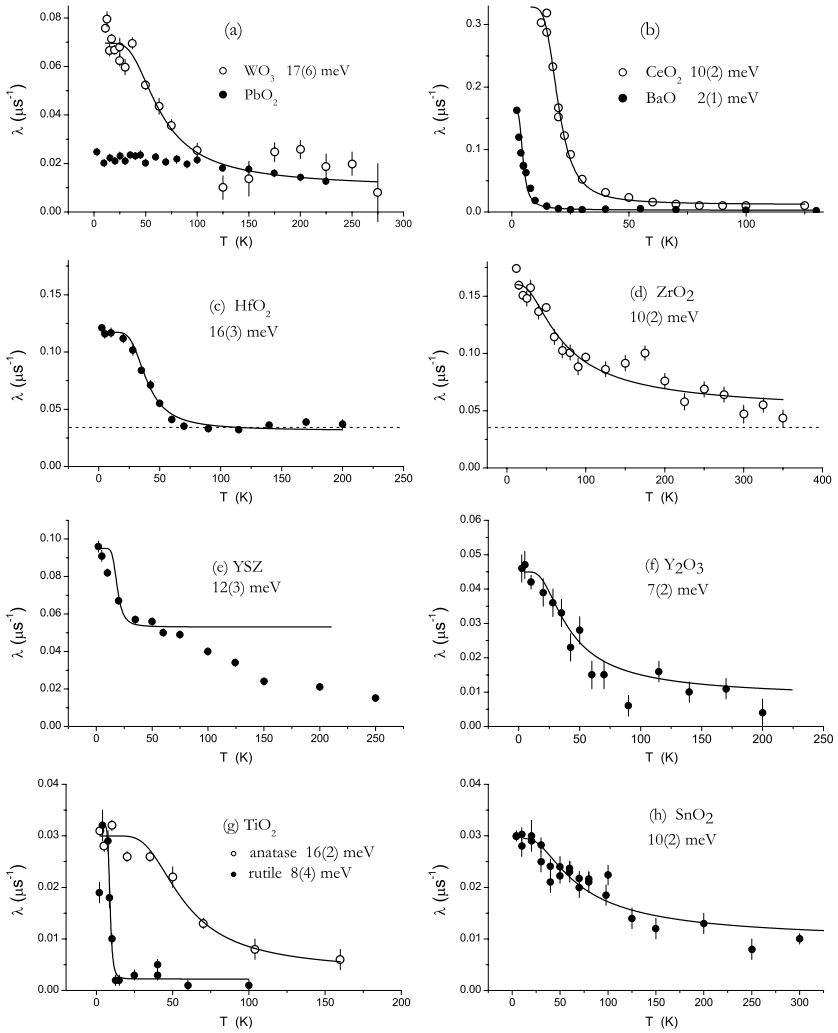

Figure 6. Lorentzian linewidth data for oxides with weak nuclear magnetism (note different scales, as appropriate). Paramagnetic contributions to the μSR linewidth are discernible at low temperature for all except PbO_2; fits with equation (17) model the disappearance of this contribution, giving activation energies as shown. The more gradual variation at higher temperatures, most noticeable for YSZ, can be attributed to motional narrowing of the nuclear dipolar linewidth. The estimated static nuclear contribution is shown as the dashed lines for HfO_2 and for ZrO_2; a slightly higher value has been set for YSZ. Experimental μSR linewidths for the corresponding pure metals, given in table 1, may also be taken as upper limits of the nuclear contributions.

impurities are invariably present in oxides, so this contribution is not in doubt; the only question is its magnitude. We envisage here chemical impurities (i.e. magnetic transition-metal or rare-earth ions) or else self-trapped electrons (that is, some fraction of cations in the wrong oxidation state, such as paramagnetic Ti^{3+} ions in TiO_2 or Hf^{3+} ions in HfO_2). The width δB of the distribution is directly proportional to x, the fraction of cation lattice sites occupied by the impurity; assuming impurities with spin $1/2$, each carrying one Bohr magneton, the

contribution to the μSR linewidth may be approximated as

$$\delta\lambda = (\gamma_\mu/2\pi)\delta B, \tag{18}$$

with

$$\delta B \sim 10\mu_B(\mu_0/4\pi)(x/d^3). \tag{19}$$

Here $\gamma_\mu = 2\pi \times 136$ kHz mT^{-1} is the muon gyromagnetic ratio and d^3 is the volume per cation site (e.g. $d^3 \approx 0.03$ nm^3 in TiO_2)[23]. A line-width or relaxation-rate increment of $\delta\lambda = 0.04\ \mu s^{-1}$, for instance, corresponding to a local field distribution of $\delta B = 0.3$ mT, would require an impurity level around 1000 ppm ($x \approx 0.001$). Chemical impurities at this level can reasonably be discounted in our samples, which are the purest available materials, whether single crystals or sputtering targets from Pi-kem, or polycrystalline powders from Alfa-Aesar (Johnson-Matthey). For instance, the analysis certificates for our samples of hafnia and yttria give the Fe impurity level as not exceeding 25 ppm and those of various other transition metals and rare earths as each not exceeding 10 ppm. There is no reason to suppose that anomalous electronic moments of the sort reported in thin-film hafnia (Venkatesan *et al* 2004) are present in our bulk samples.

The likely concentration of trapped electrons is more difficult to judge. An intriguing possibility is that there are no pre-existing paramagnetic impurities but that reaction (5) competes with the more complete delocalization of reaction (3). In other words, it is the weakly bound muonium electron which itself becomes trapped as a polaron near the muon. A large dipolar component to the hyperfine interaction could then explain why the satellites are not resolved in a powder spectrum. (More single-crystal data would be valuable here, to elucidate this.) Separations not much more than a nanometre would be required, between the muon and the centre of gravity of the electron distribution, to give the required dipolar parameters of several hundred kHz. Otherwise short spin-state lifetimes must be blamed. We note that even for the established shallow donors in CdS, CdSe, CdTe and ZnO there is a similar collapse of the spectrum in the ionization régime (Gil *et al* 2001a), as there is when the muonium centres are in communication with other shallow donors (Corregidor *et al* 2004).

Equation (19) implies that the impurity spins are frozen, i.e. have T_1 and T_2 relaxation times both much longer than the microsecond μSR timescale, as seems likely for isolated paramagnetic centres at the lower cryogenic temperatures. In this model, the reduction of μSR linewidths towards 100 K would represent the onset of impurity spin relaxation. An alternative interpretation involving rapid fluctuation of the impurity spins at all temperatures is untenable. In this model, the variation of μSR linewidth would follow Curie's law, which does not fit the data at all well. Even more pertinently, each moment would then be effectively reduced to a much smaller average value governed by thermal equilibrium electron polarization, so that an impurity concentration x close to unity would be implied. We conclude that impurity broadening is not a significant complication. The higher linewidths seen in purer samples of ZrO_2 (Amato *et al* 2003) are supportive in this respect and may be seen as an enhanced yield of the shallow-donor state.

[23] The muons are presumed to adopt well-defined positions adjacent to oxygen within each unit cell but the length-scale between impurities is much larger. The field distribution is sampled at random, therefore, and mapped as a contribution to the lineshape of the μSR spectrum, as it is in the NMR spectrum of host nuclei. Formulae given by Abragam (1961), Walstedt and Walker (1974) for NMR usage have been adapted here, rewritten for SI units and μSR linewidth λ. The numerical factor is variously given as 5–10, according to structure and the approximations used; we take the upper value to be on the safe side.

4.3. Delayed muonium formation

Before committing to the interpretation of shallow-state formation we consider one further alternative, namely whether the low-temperature linewidths could represent lifetime broadening. In particular, delayed capture of an electron to form normal or atomic muonium would cause damping of the Mu^+ Larmor-precession signal. (That is, the amplitude would decrease exponentially, as polarization is transferred incoherently to other frequencies.) The Lorentzian linewidths of figure 6 would then correspond to average electron lifetimes of 10–30 μs, which is improbable: radiolytic electrons would undoubtedly find other traps, notably vacancies, on much shorter timescales. In BaO, WO_3, TiO_2 and SnO_2, we are also able to discount such slow muonium formation by measurement of the depolarization rate in low longitudinal fields: the depolarization is entirely suppressed in a field of 10 mT or lower, whereas for normal muonium formation it would remain constant in rate (i.e. be independent of field, as for any chemical rate constant) and be suppressed in amplitude only at much higher fields. These are the materials where the muon spin rotation signal has maximum amplitude, accounting for 100% of the incoming muon polarization. For those which show reduced amplitude, e.g. HfO_2, ZrO_2 and Y_2O_3, the question is more subtle. We can again rule out slow electron capture but cannot discount the possibility that the weakly bound states are relatively long-lived precursors to atomic muonium. The relevant data, including the interesting case of CeO_2, are discussed in appendix A.

4.4. The Group IIA oxides

Early studies found normal muonium in BeO, MgO and CaO but reported no unusual or weakly bound paramagnetic states (Brewer 1983, Spencer *et al* 1984, Kiefl *et al* 1986). One might argue that stabilization of the interstitial proton by formation of hydroxide ions (reaction (3)) is least effective in those members of the family with high oxygen coordination (octahedral in MgO, CaO, SrO and BaO) so that BeO (tetrahedral) is the most likely to show shallow-donor formation. Observation of the shallow-donor signature in our spectra, not of BeO but of BaO (figure 5(a)), came something of a surprise, therefore. No previous measurements have been reported in BaO and, equally surprising, it proves to be the only IIA-oxide to show no normal-muonium fraction.

In SrO, as well as detecting normal or atomic muonium, we find that the linewidth of the Larmor precession signal increases to 0.1 MHz below 100 K. This is far greater than can be attributed to the sparse ^{87}Sr nuclear moments and so is strongly suggestive of a coexistent shallow-donor state, or of a weakly bound precursor to the normal muonium. No such indications of shallow or weakly bound state are seen either in CaO or MgO. Although the μSR linewidth is greater in BeO, it is adequately accounted for by the stronger nuclear magnetism, as is the case for most of the materials covered in the following section.

4.5. Materials with large or abundant nuclear moments

It will be more difficult to identify shallow-donor muonium states in materials where the nuclear-dipolar broadening of μSR spectrum might exceed or obscure the hyperfine splitting. This has proved possible in two of the III–V semiconductors, nonetheless—namely InN, where the satellite lines can be convincingly deconvolved, and GaN, where they are actually resolved (Davis *et al* 2003, Shimomura *et al* 2004). We present here a search in the oxides of Bi, La, Li, Nb, Sb and Ta (in the lower portion of table 1). Only in Li_2O are hyperfine satellites clearly visible in the low-temperature spectrum, disappearing towards 100 K (figures 7(a), (b)). Although the overall linewidths vary with temperature for the other materials, it is virtually impossible to distinguish electronic and nuclear contributions (figures 7(c), (d)). A case can

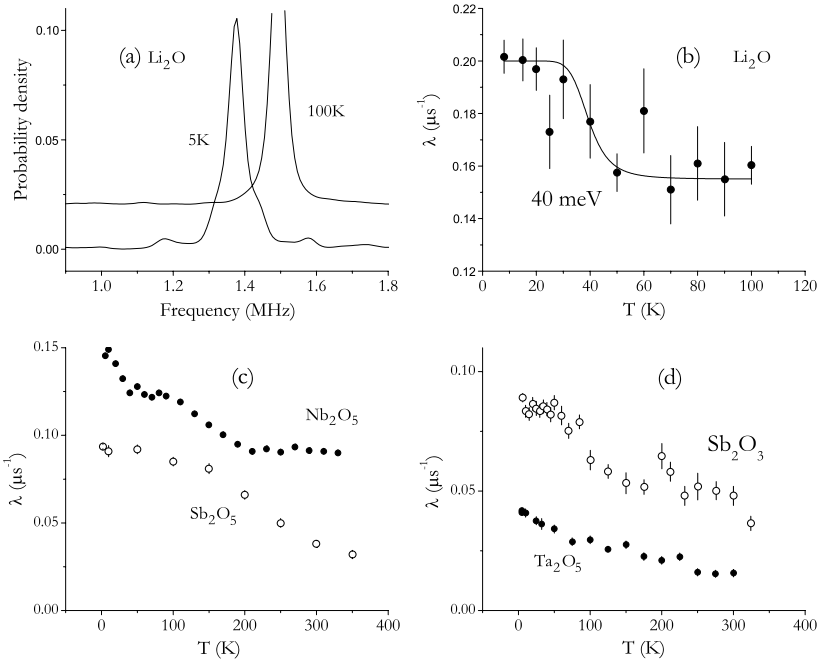

Figure 7. The shallow-donor search in materials with strong nuclear magnetism. For Li_2O, the μSR spectrum in a field of 10 mT is shown below and above the ionization temperature in (a) and the variation of overall linewidth with temperature in (b). (The 100 K spectrum is offset in (a) for clarity, there being no such actual frequency shift; equation (17) is fitted in (b), excluding the two erratic data points.) The variation of μSR linewidth with temperature is shown for materials in which hyperfine satellites are not visible in (c) and (d): there are signs of a $Mu^0_{shallow}$ contribution below 50 K in Nb_2O_5, but not in Sb_2O_5; no firm conclusions can be drawn for Sb_2O_3 or Ta_2O_5.

be made for a weakly bound or shallow-donor muonium state in Nb_2O_5, where there is an abrupt upturn of linewidth below about 50 K. Otherwise, the temperature dependences can reasonably be attributed to motional narrowing of the nuclear contribution. i.e. to the onset of muon diffusion. Thus no strong case can be made for shallow-donor muonium states in Sb_2O_3 or Sb_2O_5. For Ta_2O_5, the case is borderline: the linewidth seems curiously small, given the ^{181}Ta nuclear moments, suggesting that the muons are mobile at all temperatures. Similarly (though not shown in the figure) there is a candidate shallow-donor signature in the data for La_2O_3 but not for Bi_2O_3.

It is worth noting that the materials with pentavalent cations—Nb_2O_5, Sb_2O_5 and Ta_2O_5—show full asymmetry in the muon Larmor precession signal. That is, there is no indication of normal muonium formation in these materials. In the materials with trivalent cations, however, the Larmor precession signal shows less than full asymmetry; this suggests that Mu^0_{atomic} is important, as we confirm by another method in the following section. In appendix B, we pay particular attention to the muon response in Bi_2O_3 and Sb_2O_3, in view of persistent reports of anomalous magnetism in these traditionally diamagnetic materials.

5. Atomic muonium

5.1. The longitudinal-field signature

Of the various means of detecting and characterizing normal muonium, i.e. Mu^0_{atomic}, the best suited to our purpose is the longitudinal-field method known as repolarization (see e.g.

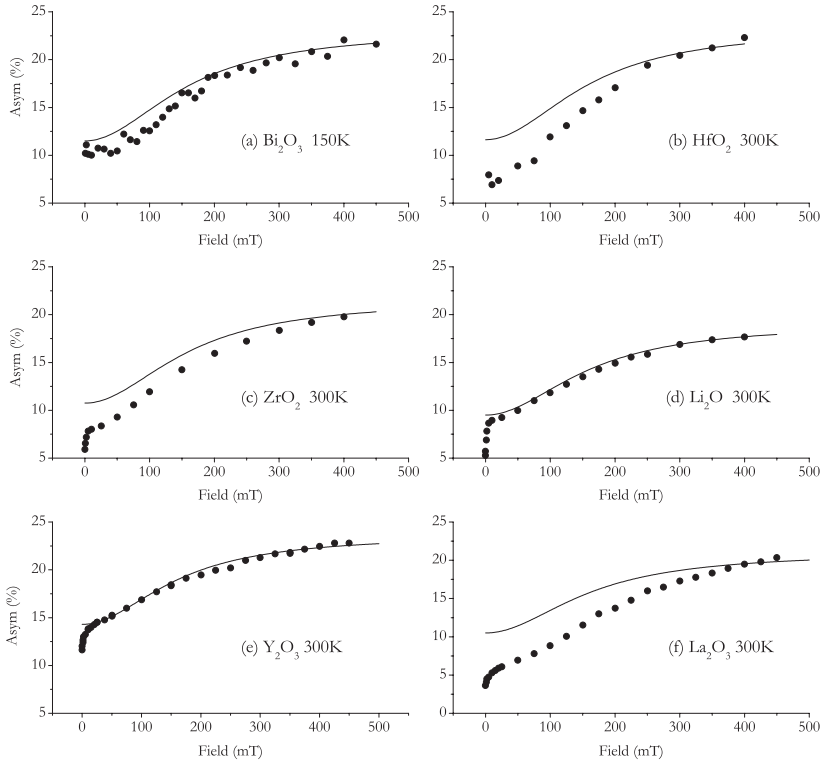

Figure 8. Longitudinal-field repolarization curves for six materials for which some polarization is missing in the transverse-field precession signals. The initial or relaxing amplitude is given here as muon-decay asymmetry—typically 24% for full polarization, including the diamagnetic background. The drawn curve is in each case that expected of free or vacuum-state muonium, scaled only in amplitude.

Minaichev *et al* 1970a, 1970b, or Patterson 1988). Forward–backward asymmetry in the muon decay is measured as a function of magnetic field applied in-line with the initial muon polarization (at ISIS, in-line with the incoming muon beam). It increases monotonically as the various terms in the muonium spin Hamiltonian are successively decoupled, dominated by the electron Zeeman energy[24]. The longitudinal-field signals show some spin relaxation, but this is not directly relevant to the present investigation: it has a very different origin to the damping of the transverse-field precession signals and relates chiefly to muonium (Mu^0_{atomic}) diffusion. For the present purpose, the important quantity is the initial asymmetry, extrapolated to within about 100 ns of muon implantation. Typical results are shown in figure 8.

The expectation for free or vacuum-state muonium is shown as the drawn curve in each frame of figure 8: the variation of asymmetry $a(B)$ with field is described by equation (20), itself entirely defined by a static spin Hamiltonian of the Breit–Rabi form (21) (see, e.g., Brewer *et al* 1975, or Patterson 1988):

$$a(B) = a_{\mathrm{D}} + a_{\mathrm{Mu}} \cdot \left\{ \frac{1}{2} + \frac{1}{2} \cdot \frac{B^2}{B^2 + B_0^2} \right\}; \tag{20}$$

[24] The resulting curves are variously known as repolarization, decoupling or quenching curves; in figure 8 we do not access the resonant dips in polarization that can occur at level crossings, though one such may be seen for GeO_2 in figure 10 and some striking examples are given for the case of silver oxide in Paper I.

$$\mathcal{H} = A\mathbf{I}\cdot\mathbf{S} - \nu_e S_z + \nu_\mu I_z. \tag{21}$$

The so-called hyperfine field is $B_0 = \pi A/\gamma_e$, which is 160 mT for an isotropic hyperfine constant of the vacuum-state value, $A = 4.5$ GHz. Departures from this value are well known in semiconductors—a value as low as $A = 1.3$ GHz in Cu_2O is reported in Paper I—but are less important in wide-gap materials (Cox 1987, 2003b); Kiefl *et al* (1986) report $A = 3.9$ GHz for muonium in MgO. In figure 8, deviations of the data from the free-atom curves are mainly due to other terms in the Hamiltonian, both static and dynamic. Thus the depolarization at low field can be attributed either to a degree of anisotropy in the muon–electron hyperfine interaction (see, e.g. Pratt 1997) or to superhyperfine interactions with adjacent nuclei (see, e.g. Beck *et al* 1975)[25]. Other distortions of the shape can occur if there is ionization or chemical conversion between muonium and diamagnetic species (Ivanter and Smilga 1968, 1969); in this case the diamagnetic and paramagnetic asymmetries, a_D and a_{Mu}, are not constants in equation (20) but reflect the competition between field-dependent spin–lattice relaxation and field-independent chemical conversion (see, for instance Cox *et al* 1997).

Even if equation (20) does not model the data of figure 8 accurately, the point here is that the polarization which is missing from the transverse-field precession signals for these materials is entirely accounted for by muonium with close to free-atom character, whether it be formed promptly on implantation or by delayed capture of radiolytic electrons. We find similar repolarization behaviour in Al_2O_3–sapphire and in MgO, confirming early reports of normal muonium in these oxides (Minaichev *et al* 1970a, 1970b, Spencer *et al* 1984, Kiefl *et al* 1986). We examine the deviations from the standard form for SiO_2 more carefully in section 6, below.

In figure 8 we include identification of Mu^0_{atomic} in Li_2O, this material being one of the few binary oxides besides SiO_2 in which H^0_{atomic} is known to ESR spectroscopy (Baker *et al* 1991). Apart from being a prototypical ionic conductor, its potential importance is in the nuclear rather than the electronics industry, in which context the stability of neutral atomic states of both muonium and hydrogen, up to room temperature at least, may contradict predictions for the heavier isotope tritium: Kudo and Okuno (1986), Shah *et al* (1995) expect only the positive ion to be thermodynamically stable. A proportion of the tritium released by neutron irradiation of Li_2O is known to be in the neutral state, however, and our own observation of a large atomic muonium fraction adds to the debate over the relative importance of T^0 and T^+ diffusion in tritium release from this material (Shluger *et al* 1991)[26]. Tanigawa and Tanaka (2002) suggest that protons may be trapped and reduced by F^0 centres, thereby stabilizing neutral atomic hydrogen.

The diamagnetic muonium fraction is itself of interest in Li_2O: Lord *et al* (1998) report μSR measurements that can distinguish the Mu^+ and Li^+ diffusion, setting in respectively around 80 and 250 K: they also report a similar behaviour of Mu^+ and Mu^0_{atomic} fractions in Na_2O. There is some evidence of Mu^+ trapping at cation vacancies at the higher temperatures, in which case the interstitial muon is stabilized simply by the favourable Madelung potential, i.e., without process (15). Tanigawa *et al* (2004) similarly report vacancy-trapping of deuterons. By implication, protons (intermediate in mass between muons and deuterons: $m_\mu{:}m_p{:}m_d{:}m_t =$

[25] It is exactly these other terms, or else delay to the electron capture, which can prevent observation of the muonium precession frequencies in low transverse field. The so-called triplet–muonium precession signal, characteristic of muonium in quartz, is in fact not visible for any of the materials of figure 8—whence the utility of longitudinal-field detection. The data of figure 8 are all recorded above 100 K, so the low-field repolarization is not from shallow-donor signals.

[26] The radiolytic conditions are somewhat comparable for the formation of muonium and tritium, but not for their diffusion and trapping: the incoming muons each carry 4 MeV, compared with 2.7 MeV for tritons from the $^6Li(n,\alpha)T$ reaction, but the lighter muon mass means less structural radiation damage as well as fast diffusion away from the damaged area.

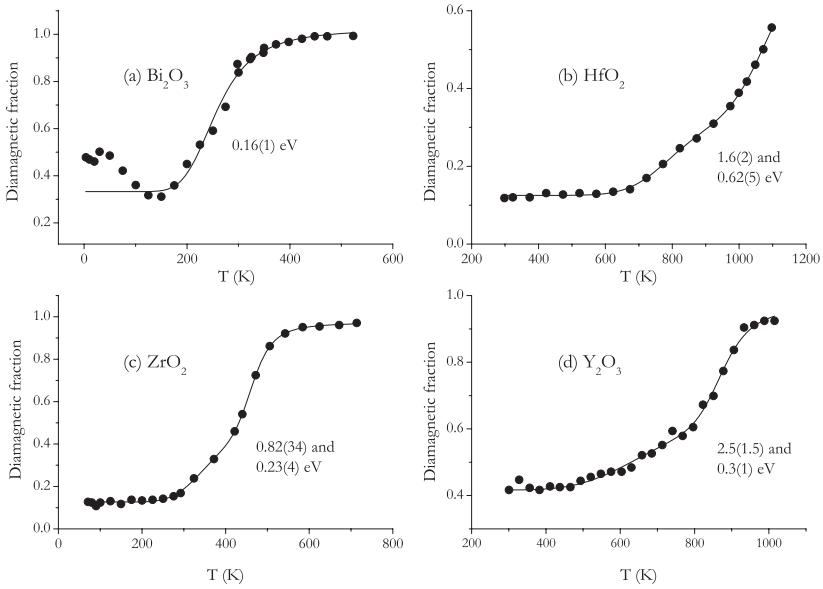

Figure 9. Disappearance of normal muonium at high temperatures, as monitored by the recovery of the diamagnetic fraction towards unity. For Bi_2O_3 (a) the variation below room temperature is similar to that reported by Duginov *et al* (1994b). For HfO_2 (b) conversion is not complete at the furnace temperatures accessible to us. The fitted curves in the linear plots (a)–(c) use expression (16) or a two-step version of this, as indicated. The fitted activation energies may define deep acceptor levels, as depicted in (d), or else barriers to site change—see figure 12(b).

$\frac{1}{9}$:1:2:3) may also be stabilized in cation vacancies without bonding to oxygen, i.e., without process (2).

For the candidate high-permittivity dielectrics such as ZrO_2 and HfO_2, the existence of Mu^0_{atomic} is another aspect relevant to a full description of electrical activity of hydrogen impurity, as we discuss in the following section.

5.2. High-temperature ionization of normal muonium

It is worth drawing attention to the remarkable stability of normal muonium in quartz: in our own measurements, a muonium signal (the so-called triplet precession signal in weak transverse field) is still visible in fused silica at 1100 K; for crystalline quartz, Dawson *et al* (1997) report that the signal persists to 1250 K. More usually, the muonium fraction varies considerably with temperature. Small variations at cryogenic temperatures must relate to the precise mechanism of electron capture but a common feature of our oxide data is the loss of the paramagnetic fraction towards or above room temperature. There is a concomitant rise of the diamagnetic fraction which is shown for three materials in figure 9. For Bi_2O_3 and ZrO_2 the conversion is essentially complete by 600 K and for Y_2O_3 by 1100 K but for HfO_2 the diamagnetic fraction is still growing at this temperature. The difference in behaviour between HfO_2 and ZrO_2 is somewhat surprising, given their chemical similarity. Since these are defective materials, artefacts of muonium diffusion and trapping cannot entirely be ruled out (cf reactions (7) and (8) for H in HfO_2); in the following, nonetheless, we pursue models of charge-state transitions at intrinsic interstitial sites. It is unlikely that the various forms of ionic conduction exhibited by these materials at high temperatures (typically towards their melting points) influence the muonium data.

The disappearance of atomic muonium and corresponding recovery of the diamagnetic signal is evidently thermally activated and is reasonably well described by equation (16). It is tempting to associate the transition with a deep-acceptor function, i.e. to suppose that Mu^0_{atomic} disappears at high temperature by hole ionization, $Mu^0 \rightarrow Mu^- + h$ (cf. process (10) for hydrogen). In this model, the high-temperature state is the negative ion and the activation energies would represent the heights E_A of the deep $(0/-)$ acceptor levels above the valence-band maxima. Better fits are obtained with two-step versions of equation (16), as shown for the other materials in figures 9(b)–(d): the activation energies are 0.6 and 1.6 eV, for HfO_2, 0.2 and 0.8 eV for ZrO_2, and 0.3 and 2.5 eV for Y_2O_3. The latter value of 2.5 ± 1.5 eV for Y_2O_3 would, despite its imprecision, be consistent with an acceptor level near midgap ($E_g = 5.9$ eV in this material). It is also noteworthy that Y_2O_3 is one of the few materials in which H^- is calculated to be the stable charge state (Ragnarsson *et al* 2001). For Bi_2O_3, ZrO_2 and HfO_2—we have not yet examined the high-T disappearance of muonium in other materials—assignment of the activation energies to acceptor levels would place these low in the gap. An alternative possibility is mooted in the concluding section, namely a site-change combined with electron ionization. If the two activation steps refer to independent processes in each case, it may even be that conversions to the positive and negative ion are both important.

Unfortunately, identification of the high-temperature ionic state will be difficult, since both Mu^+ and Mu^- may be expected to diffuse rapidly at such high temperatures. Even in Bi_2O_3, where the nuclear moments are large, no increase of μSR linewidth at high temperature is seen, as might be expected for Mu^- adjacent to cations; on the contrary, the linewidth is reduced by motional narrowing, so that site and charge-state remain indeterminate.

6. Muonium–vacancy complexes in germania and silica

6.1. Transverse-field versus longitudinal-field spectroscopy

The reported muonium spectrum in SiO_2 has essentially free-atom character and undoubtedly represents muonium located in interstitial cages in undefective regions of the host lattice: just a small degree of anisotropy is detectable in the hyperfine parameters, varying according to whether the muonium is static or diffusing (Brewer 1981). The same is true of atomic hydrogen in quartz—one of the relatively few examples of interstitial H^0_{atomic} detected in an oxide by ESR spectroscopy. Both the μSR and ESR measurements have been made to sufficient precision to discuss the effects of interstitial confinement, as well as the resultant small isotope effect arising from the different zero-point motions of muon and proton (Weil 1981). But for our purposes, the contact interactions may be considered equal to the respective vacuum-state values. Normal muonium is likewise reported in GeO_2, but only with a yield that is low ($\leqslant 16\%$, per implanted muon) and sample dependent (Spencer *et al* 1984). Much of the muon polarization is unaccounted for in the muon spin rotation spectrum for GeO_2 although Brewer (2002) reports unassigned frequencies. Inspired by this, we have undertaken a longitudinal-field study—with surprising results, both in GeO_2 and SiO_2.

Figure 10(a) shows our repolarization study for GeO_2, in which the polarization which is missing in transverse-field spectra is largely recovered in a longitudinal field of 0.4 T. The model curve shown as the dashed line is simulated for a single anisotropic muonium state with axial symmetry. The contact term of $A_{iso} = 56$ MHz and dipolar term of $D = 42$ MHz (with opposite signs) recall remarkably similar values for anomalous or bond-centred muonium in the elemental semiconductors, namely $A_{iso} = -67$ MHz and $D = 51$ MHz in Si, $A_{iso} = -96$ MHz and $D = 69$ MHz in Ge (Cox and Symons 1986). The local electronic structure must be extremely similar, exhibiting a node in electron density at or close to the

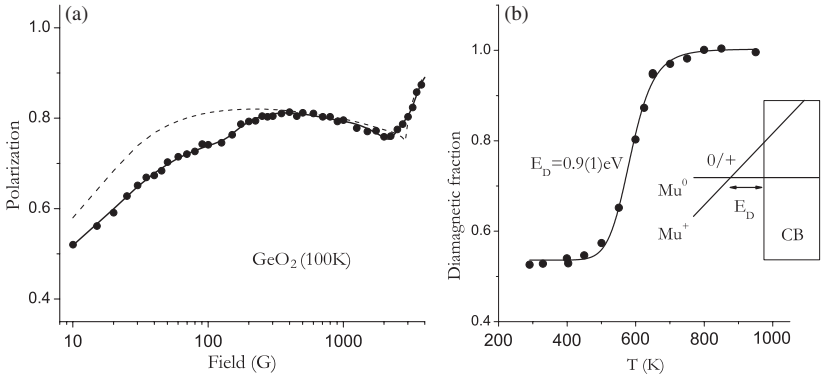

Figure 10. Characterization of the muonium state in GeO_2 by means of its repolarization (a) and ionization behaviour (b). The dashed line in (a) is a simulation for an axially symmetric hyperfine tensor, not unlike that of Mu_{BC} in elemental Ge; the full line a fit for a rhombic centre with shallow precursor. The curve in (b) is fitted using equation (16), with the activation energy taken to define a deep-donor level E_D, referred to the conduction band minimum (compare the sketch in (b) with figure 1).

muon site. However, this model over-emphasizes the sharpness of the cusp—the level crossing resonance near 200 mT—and a more satisfactory fit is obtained when this muonium state is allowed complete anisotropy: the contact and dipolar terms remain similar but there is an additional *x*–*y* anisotropy of 43 MHz, leading to principal values of 15, 58 and 90 MHz. This is the solid curve in figure 10(a)[27].

Figure 10(b) shows the ionization behaviour: the diamagnetic fraction reaches unity by about 800 K and the fitted curve here uses equation (16) to yield an activation energy of 0.9 ± 0.1 eV. Despite the large value, we assign this to a donor depth, referred to the conduction band minimum as sketched in the figure. The deep-donor behaviour is well established for anomalous or bond-centred muonium and the analogous hydrogen state in Si: for these the donor depths are close to 0.2 eV, with a small but calculable isotope effect (Cox 2003a). Amongst the other oxides, the closest analogy is with the deep-donor state of muonium in HgO, for which the hyperfine parameters are not dissimilar and the effective ionization energy is 0.15–0.3 eV (Gil *et al* 2001b, Cox *et al* 2001b).

6.2. The vacancy complex and bridging site

Although we have no site determination yet, there is little doubt that this novel muonium centre in germania is the counterpart of the E_4' centre in quartz, known from ESR spectroscopy to be hydrogen occupying an oxygen vacancy (Isoya *et al* 1981). The hyperfine parameters, scaled appropriately, are virtually identical and the bridging site between Si or Ge atoms explains the resemblance to bond-centred muonium in elemental silicon or germanium. What is curious is that this appears to be the dominant muonium centre in the oxide germania but that its equivalent in silica has not been reported. As a minority component, or one that is not formed promptly on muon implantation but rather by diffusion and trapping of normal muonium, it

[27] The simulation and fitting of repolarization curves and level crossing resonances, including the effects of state conversion and spin dynamics, is described elsewhere (Lord 2006). Here some unidentified dynamics appears to distort the curve at lower field: although this may be fitted by invoking conversion to a state with even lower hyperfine parameters, in the vicinity of 1 MHz, it seems unlikely that a shallow state would persist to 100 K, where these data were recorded. The alternative model of conversion *from* the shallow state does not fit quite as well, but recalls the contention of Storchak *et al* (2004), namely that electrons may be captured first into weakly bound excited states, subsequently cascading to more localized deep centres.

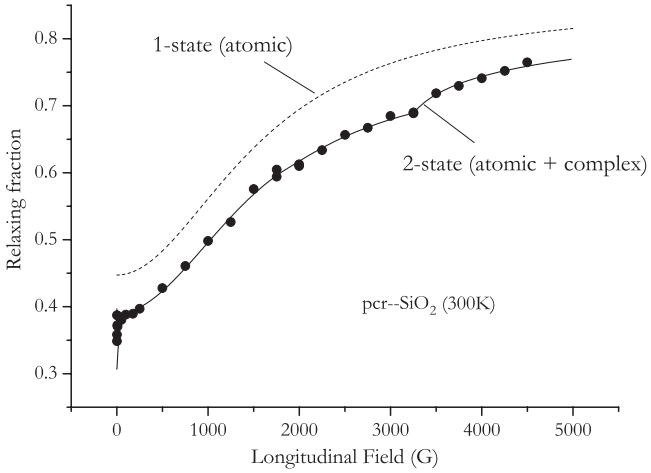

Figure 11. Repolarization in polycrystalline quartz at room temperature. The data set is the relaxing asymmetry, fitted assuming isotropic muonium with atomic character, together with a highly anisotropic muonium state, as described in the text. Spin–lattice relaxation is weak except at the lowest fields so that the same curve describes the time-integral muon polarization (the latter offset by a small diamagnetic signal). The standard curve for atomic muonium alone is drawn for comparison as the dashed line according to equation (20); it is given the vacuum state hyperfine field of 1600 G ($A = 4.5$ GHz), fitted only in amplitude and displaced for clarity.

could well have gone undetected. We show in figure 11 that when the repolarization curve is recorded in sufficient detail (here for a polycrystalline quartz sample) it does indeed show deviations from the standard form of equation (20). The fitted solid curve in figure 11 has 12% of the neutral muonium fraction with axial hyperfine parameters $A_{\rm iso} = 76 \pm 2$ MHz and $D = 24 \pm 5$ MHz, with opposite signs. Scaled for hydrogen, these become $A'_{\rm iso} = 24$ MHz and $D' = 7.5$ MHz; the corresponding values measured for the E'_4 centre at room temperature (Isoya *et al* 1981) are 18 MHz (0.65 mT) and 17 MHz (0.62 mT), respectively.

It is noteworthy that muonium–vacancy complexes in elemental silicon were discovered in the same way, with hyperfine parameters from careful repolarization studies matching those from ESR spectra of hydrogen–vacancy complexes (Schefzik *et al* 1998, 2000, Bech Nielsen *et al* 1997). In the present case, we envisage the vacancies to be pre-existing, rather than created by the particle implantation; if so, the yield of the new centre in quartz is likely to be sample dependent—as indeed is the diamagnetic Mu^+ fraction (Catlow *et al* 1995)—though we have not yet pursued this. While we do not exclude the possibility of similar components in the repolarization curves of figure 8, their departure from the purely atomic form is not so distinctive or readily fitted.

7. Summary and concluding remarks

7.1. The shallow states: hydrogenic versus polaronic models

Table 2 gives a compendium of all paramagnetic muonium states found so far in non-magnetic binary oxides, including results from the accompanying Paper I and older μSR literature. Shallow-donor states are observed or are inferred with reasonable confidence in BaO, CeO_2, CdO, HfO_2 (monoclinic), Li_2O, SnO_2, SrO, TiO_2 (both anatase and rutile), WO_3, Y_2O_3, ZnO

Table 2. Results for neutral (paramagnetic) muonium states. The designation Shallow Donor implies direct observation or reasonable inference; candidate shallow donor (SD) indicates that the current results are suggestive but not conclusive. The designation atomic implies a hyperfine constant within about 20% of the free-atom value; in the quasiatomic state in Cu_2O it is reduced by 70%. Contact terms for the shallow donors are inferred to be smaller by 4 or 5 orders of magnitude, with indeterminate sign; their effective ionization energies are given in table 3. The deep-donor states have hyperfine parameters that are intermediate in value and highly anisotropic. References or notes: [I] = accompanying paper; [2] Brewer (1983); [3] Brewer *et al* (2000); [4] Cox *et al* (2001b); [5] Spencer *et al* (1984); [6] Kiefl *et al* (1986); [7] Brewer (1981); [8] Cox *et al* (2001a); [9] Shimomura *et al* (2002). Band-gap and oxygen coordination for the host materials are tabulated (from literature compilations) to aid the search for systematics: see also table 3 and figure 13.

	Muonium category	Ionization range (K)	Fraction at RT	Reference or notes	Bandgap E_g (eV)	Oxygen coordn.
Ag_2O	1. Candidate SD	125–250		[I]	1.2–1.6	4
	2. Deeper precursors			[I]		
Al_2O_3	Atomic		0.35	App. A.3	8–9	4
BaO	Shallow donor	2–30			4.4	6
BeO	Atomic		0.2	[2]	9–11	4
Bi_2O_3	Atomic	150–450	~ 0.25	[I]	1.6–3	4
CaO	Atomic	>300	0.35	[2]	7–7.8	6
CdO	Shallow donor	100–200		[I]	0.6–0.8	6
CeO_2	Shallow donor	15–50			4–4.5	4
Cu_2O	Quasiatomic	650–900	0.7	[I]	2–2.8	4
GeO_2	Deep donor?	500–800	0.45		5.6–6	2
HfO_2 (m)	1. Atomic	700–1000+	~0.8		6	3, 4
	2. Shallow donor	5–100				
HgO	Deep donor?	100–200		[4]	2.2	2
La_2O_3	1. Atomic	>300	~0.8		6	4, 6
	2. Candidate SD	5–25				
Li_2O	1. Atomic	>300	~0.5		6.6–7.7	8
	2. Shallow donor	30–70				
MgO	Atomic	>300	0.15	[5, 6]	7.7–7.9	6
Nb_2O_5	Candidate SD	10–50		4		2, 3
PbO(t)	None			[I]	1.9	4
PbO_2	None				4.5	3
Sb_2O_3	Atomic	>250	$\leqslant 0.6$		3.3	2, 3
Sb_2O_5	None					2, 3
SiO_2	Atomic	>1000	0.6	[5,7]	8.9	2
SnO_2	Shallow donor	20–150			2.7	3
SrO	1. Atomic	>300			5.3–6.4	6
	2. Shallow donor	50–150				
Ta_2O_5	Candidate SD	5–100			4.4	2, 3
TiO_2 (anatase)	Shallow donor	50–100			3.1	3
TiO_2 (rutile)	Shallow donor	5–20			4	3
WO_3	Shallow donor	10–80			2.6–2.9	2
Y_2O_3	1. Atomic	500–1000	0.6		5.9	4
	2. Shallow donor	10–100				
ZnO	Shallow donor	30–50		[8,9]	3.4	4
ZrO_2 (m)	1. Atomic	300–600	0.8		5.5–5.8	3, 4
	2. Shallow donor	10–100				
ZrO_2 (c/YSZ)	1. Atomic	>300	~0.2		5.7	4
	2. Shallow donor	10–100				

Table 3. Comparison with the hydrogenic model, for muonium shallow donors and candidate shallow donors. Electronic parameters, where available, are used with equation (4) to predict shallow-donor binding energies R^* or to estimate the missing effective masses m^*. Our experimental activation energies—the effective muonium ionization energies—are taken from figures 6, 7, A.1, A.2 or from Paper I and have accuracies typically no better than 50%; no reliable estimates can be made for La_2O_3, Nb_2O_5 or Ta_2O_5. (Dielectric constants and effective masses are cited from [1] Houssa (2004), [2] Madelung (1996, 1992), [3] Stoneham and Dhote (1997), [4] Wuilloud *et al* (1984) (the appropriate sub-gap is given—see section 7.5), [5] Ong (1983), [6] Osaka and Shindo (1984), [7] Rignese (2005, plus references therein), [8] Hjelm *et al* (1996).)

	$\varepsilon_r(\omega \to 0)$ $= \varepsilon_r$ (static)	$\varepsilon_r(\omega \to \infty)$ $= n^2$ (optic)	m^*/m_e	Ref.	R^* from equation (4)	Activation energy (eV)	m^*/m_e from present data
Ag_2O			0.7	[2]		0.13 [I]	
BaO	34	3.6	0.59	[2]	0.007	0.002	
CdO	22	5	0.11	[2]	0.06	0.05 [I]	
CeO_2	12–20			[4]		0.03	0.3–0.9
m–HfO_2	15–26	6		[1, 3]		0.02	0.4–1.1
La_2O_3	21–30	4		[1]			
Li_2O	8.1	2.7		[5, 6]		0.04	0.2
Nb_2O_5	11–14			[1]			
SnO_2	10–14	4	0.3	[3]	0.02	0.01	
SrO	13–15	3	0.54	[2]	0.04	0.03	
Ta_2O_5	25	4		[1]			
TiO_2 (anatase)	86–170	7–8		[3, 7]		0.02	10–40
TiO_2 (rutile)	50–80	4		[1]		0.01	2–5
WO_3	10–14	4		[8]		0.02	0.2
Y_2O_3	12–18	3		[1, 3]		0.07	0.7–1.6
ZnO	8	4	0.24	[2]	0.05	0.03	
m-ZrO_2	14–25	5		[1]		0.02	0.3–0.9
c-ZrO_2 (YSZ)	27–29			[1, 7]		0.01–0.03	0.5–1.8

and ZrO_2 (both monoclinic and cubic)[28]. Not all of these show resolved hyperfine satellites in the μSR spectra but the linewidth data alone are sufficiently compelling. Indications of such states are also found in La_2O_3, Nb_2O_5 and Ta_2O_5 but, for these, uncertainties over the nuclear line-broadening make the present data less conclusive; we designate them 'candidate shallow donors' in table 2.

The term shallow donor is used here to mean a paramagnetic centre in which the electron orbital can be described by effective-mass theory. This is difficult to verify, since only for a few oxides have electron effective masses been reported. A compilation of the relevant parameters is given in table 3, where our experimental results for apparent ionization energies are compared, where possible, with the predictions of equation (4). There is reasonable agreement for ZnO, SnO_2 and SrO. There is apparent agreement for CdO only if the high-frequency permittivity is used in equation (4), as discussed in Paper I; this substitution does not resolve the discrepancy for BaO, however, suggesting that other corrections are needed to the simple hydrogenic theory[29]. The question as to whether the much larger donor depth of

[28] The cubic or antifluorite ZrO_2 here is YSZ, i.e. yttria-stabilized zirconia, our sample containing 9.5 at.% Y_2O_3; it is the polymorph with the largest bandgap. YSZ being a standard proton conductor, the intriguing implication is that hydrogen impurity may induce both protonic (p-type) and electronic (n-type) conduction!

[29] Recalling the discussion for ZnO in section 3.1, the donor depths may equate to twice the measured ionization energies, according to the nature of the local equilibrium. More generally, the hydrogenic or effective-mass theory assumes a spherically symmetric and Coulomb potential centred on the defect site. Any deviations from the latter necessitate the inclusion of so-called central-cell corrections in the evaluation of binding energies and are normally required for shallow centres in semiconductors. Even acknowledging that muonium (or hydrogen) has no core electrons, the potential in which the bound electron moves must deviate from being coulombic in the vicinity of the muon (or proton). The shallow-to-deep instability is itself the extreme manifestation of the breakdown of effective-mass theory.

0.25 eV, for the muonium state designated Mu^I in Ag_2O, qualifies as shallow in this sense is also discussed in Paper I. Dielectric constants being known for most oxides, we use our muonium activation energies in conjunction with equation (4) to deduce the missing electron effective masses, entered in the last column of table 3. The values for the most part seem physically reasonable, the larger values (especially for TiO_2) conceivably representing polaron masses.

The lack of resolution of the hyperfine satellites in our spectra could represent considerable anisotropy in the hyperfine tensors, consistent with polaronic models (see figure 1 (c)), electron distributions centred a short distance away from the muon site giving the requisite dipolar terms. Alternatively, the lack of resolution may simply be due to short spin-state lifetimes in the shallow-donor states, on the microsecond or immediate sub-microsecond range. Data for CeO_2, presented in appendix A.2, suggests the possible combination of both effects, namely spin exchange on a highly anisotropic polaronic centre. Our estimates of donor depth and effective mass fail if the spin exchange arises from ionization of other shallow centres or if the μSR linewidths collapse not by ionization but by spin–lattice relaxation. In this latter case, the activation energies refer not to the full donor depth but to some smaller splitting of the donor level, so the value appropriate to carrier activation is underestimated.

7.2. Trapped-atom states: deep acceptors versus deep donors

In contrast to the extended orbitals of the shallow states, highly localized muonium states with trapped-atom character are formed in Al_2O_3,[30] BeO, Bi_2O_3, CaO, HfO_2, La_2O_3, Li_2O, MgO, SiO_2, SrO, Y_2O_3 and ZrO_2. In HfO_2 and ZrO_2, therefore, as well as in Li_2O, the atomic and shallow-donor states coexist at low temperatures. The same is probably true in Y_2O_3 and La_2O_3. Normal muonium, mimicking the trapped-atom state of hydrogen, persists to considerably higher temperatures than the neutral shallow donors—typically at least to room-temperature and in some cases much higher. It has close to free-atom character in these wide-gap oxides but in semiconducting Cu_2O has a hyperfine constant only 30% of the vacuum-state value (Paper I).

Given the various theoretical predictions that hydrogen should constitute a negative-U system in many oxides—perhaps all—these observations of atomic muonium in its neutral paramagnetic state are at first sight surprising. They indicate stability of the compact singly occupied orbital, or at least its metastability on the microsecond timescale. The fact that atomic hydrogen is likewise seen by ESR in quartz may well mean that the lifetimes are longer still. It is well known that the neutral state of negative-U defects can be regained under conditions of illumination and it could be that radiolytic conditions are similarly responsible, both for the μSR and ESR observations[31]. Certainly in the μSR case the individual muonium atoms are isolated, so that their stability must be discussed in relation to equation (3), not equation (6). Nonetheless, our data raise the question of whether equilibrium models of the electrical activity of hydrogen are entirely appropriate, or at what concentration of hydrogen they may become so.

7.3. Comparison with predictions

The question of the agreement or otherwise between our findings and the various theoretical predictions is not a straightforward one, since few of the theoretical predictions tackle the questions of metastability or coexistence. There is a good correspondence between our observation of shallow-donor muonium states and all predictions of the band-resonance of hydrogen single-particle levels, namely in WO_3 (Hjelm *et al* 1996), in HfO_2, ZrO_2, SnO_2,

[30] This is established for sapphire (Minaichev *et al* 1970a, 1970b) but, given the data of Boekema *et al* (1986), is probably also true of corundum.

[31] We do not subscribe to the view of Blöchl (2000), who asserts that it is simply a consequence of large $|U|$.

TiO_2, Y_2O_3, and possibly also in La_2O_3 (Gavartin *et al* 2005, Peacock and Robertson 2003, Shluger *et al* 2003, Robertson 2004).

Correspondence with the pinning models of Kılıç and Zunger (2002) and of Van de Walle and Neugebauer (2003) is at first sight largely successful. Referring to figure 3(a), shallow muonium states are indeed seen in ZnO, CdO and SnO_2, i.e. in those materials where the pinning level has been calculated explicitly to be band-resonant. Referring to figure 3(b), where it is extrapolated onto electrochemical data, shallow states are seen in ZrO_2, Nb_2O_5, TiO_2 and WO_3, but our data are inconclusive for Ta_2O_5 and Sb_2O_3. (This latter certainly exhibits an atomic muonium state, if not also a shallow one.) The case of HfO_2 is clearly borderline, and we find deep and shallow states coexisting. In HgO, the anomalous muonium centre has hyperfine parameters characteristic of a compact centre, i.e. one which is by definition deep (Cox *et al* 2001b); however, since it is ionized at room temperature, with no sign of a compensating acceptor state, the distinction with a shallow donor is academic in this case. A notable exception to the predictions of figure 3(b) is the case of Bi_2O_3, where we find the trapped-atom rather than the shallow-donor state. (If the pinning model is valid, therefore, the electrochemical band-offset data must be in error for this material.) Although we contest the prediction for PbO_2, in this wide-gap material we find no paramagnetic muonium of any description, deep or shallow, down to 2 K. This may be simply a problem of sample condition or purity. Likewise no paramagnetic muonium states were found in semiconducting PbO and none expected or found in metallic RuO_2 (Paper I).

Despite the elegance of the pinning model, there are several conceptual difficulties in confronting it with experiment. The first applies generally and is the sparsity and acknowledged uncertainty in data for electron affinity. The second applies specifically to magnetic resonance spectroscopy, whether ESR or ENDOR for hydrogen itself or μSR for muonium. Here the principal information is on the various neutral paramagnetic states and their binding or ionization energies: yet implicit in the pinning model is the assumption that the neutral states are never thermodynamically stable. The calculations for H in MgO (Kılıç and Zunger 2002) and in SiO_2 (Yokozawa and Miyamoto 1997, Blöchl 2000, Van de Walle and Neugebauer 2003), for instance, have to be reconciled with the fact that atomic muonium is detected in its neutral state in both these materials. We address this topic in the final sections, below.

7.4. The question of metastability or coexistence

A simple representation of the deep-to-shallow instability, and the associated interplay of site and charge state, is given in figure 12. This depicts potential wells in which the neutral atomic state and the negative ion are assumed to adopt a symmetric interstitial site, e.g. a cage or channel centre, and the positive ion a hydroxide site adjacent to oxygen[32]. Frame (a) describes reaction (3), in the case that there is no barrier to release of the electron. This is the condition for auto-ionization at ordinary temperatures and for observation of a shallow-donor at cryogenic temperatures. Figure 12(b) depicts conditions for the metastable atomic state to be observed, coexisting with the positive ion or with the neutral shallow donor: the relevant potential minima must be similar in energy or else a significant barrier must exist between them. We suggest that this is the situation in HfO_2 and ZrO_2.

The question then arises whether the atomic state disappears at high temperature by conversion to the negative ion (the acceptor transition labelled E_A in figure 12(b)) or to the positive ion (over the barrier denoted E_B). The former represents hole ionization, in which case E_A is a measure of the height of the $(0/-)$ acceptor level above the valence-band

[32] The weakly bound neutral at the hydroxyl site is not depicted. We assume that the hydride ion or its Mu^- counterpart will adopt the same cage-centre sites as the neutral atoms, given their sheer size, although the conclusions are unchanged if they find sites closer to particular cations.

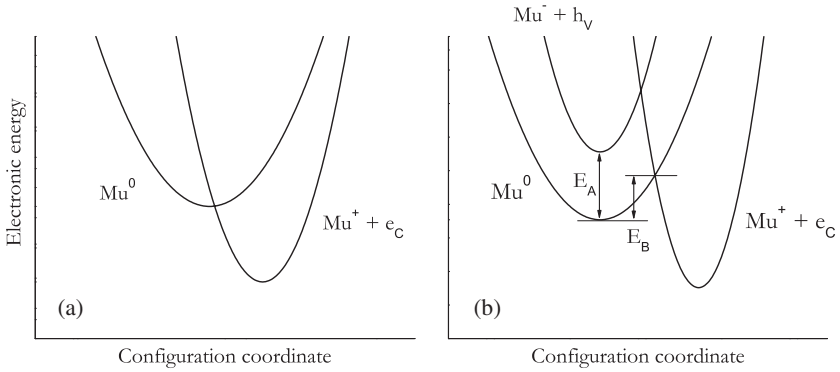

Figure 12. Potential-well diagrams for the interplay of site and charge state. The configuration coordinate corresponds to the path for reaction (3), taking a proton from a symmetric or cage-centred interstitial site to its position in a hydroxide ion, with associated lattice relaxations. In (a), this reaction proceeds with no barrier. In (b), it competes with reaction (10). (Neutral systems with the same total number of electrons are compared, in these qualitative sketches, by adding charge carriers at band edges, as indicated; this procedure obscures the variation of energy with Fermi level for the charged defects—compare figure 2.)

maximum. Hole ionization (reaction (10)) is more plausible than second electron capture (9) since, with the exception of Y_2O_3, the activation energies are less than half the band gap. Our values of 0.6 and 1.6 eV in HfO_2 may be compared here with the 2.1 eV calculated by Kang *et al* (2004). However, coexistence of a shallow-donor state in HfO_2 indicates that the $(0/+)$ donor level lies at or above the conduction-band minimum. By implication, $|U| = |E(0/-) - E(0/+)| \geqslant E_g - E_A \approx 4$ eV, which seems excessive in view of the predictions of $|U| = 1.6$ eV (Kang *et al* 2004), or even $|U| = 2.7$ eV (Gavartin *et al* 2005). Our data would imply a similarly large value for ZrO_2. Also by implication, the high-temperature diamagnetic state would be Mu^-, i.e. the hydride-ion analogue, but this has yet to be demonstrated. From this reasoning, we judge that thermal conversion to the positive ion is the more likely. In that case, the atomic states effectively act as deep donors, with site-change the bottleneck to electron release. If this is so, the deep-acceptor levels remain undetermined, as do the elusive U parameters.

The need for two distinct activation energies to describe the disappearance of atomic muonium at high temperature remains to be explained. Independent conversion to the positive and negative ions is a hypothesis to be considered. Apart from indirect evidence in Al_2O_3 and Y_2O_3, however, μSR spectroscopy as yet provides no corroboration of the rôle of hydride ions in oxide electronics.

7.5. Correlation with band-gap and the three-Δ model

In view of these uncertainties, it is valid to seek a framework for the systematics of the deep-to-shallow instability in terms of material properties that are both widely and reliably known. Figure 13 reveals—for the transparent binary oxides at least—an interesting correlation with band-gap. Materials with gaps in excess of 7 eV show only normal or atomic muonium, those with gaps between 5 and 7 eV show both atomic and shallow states—examples of coexistence or metastability which have yet to be addressed in theoretical treatments; shallow states appear to be favoured in oxides with gaps lower than 5 eV. Exceptions to this correlation are the semiconductors Ag_2O and Cu_2O of Paper I, where the proximity of cation d orbitals to the

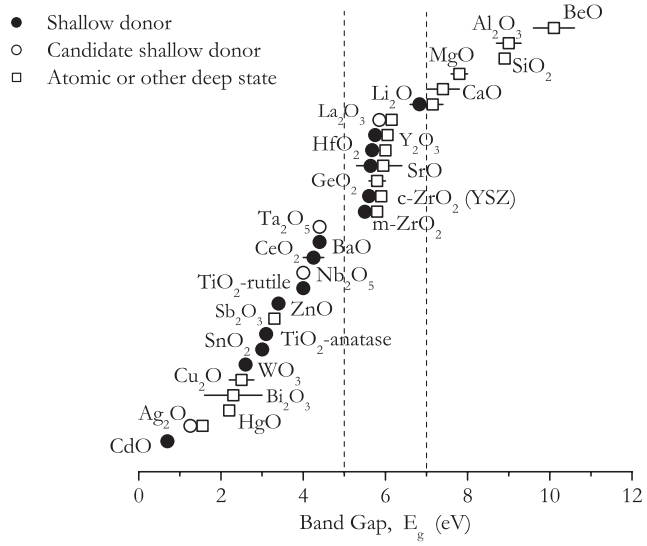

Figure 13. Muonium character versus host band-gap, plotted from table 2. A correlation emerges above about 2.5 eV, with double symbols indicating coexistence of deep and shallow states. (The horizontal bars indicate uncertainty in band gap, or its spread between polymorphs; the ordinate is purely an entry number, for display purposes.)

valence band (which otherwise has anion character) may be an issue, and likewise for several oxides with heavy-metal cations, HgO, Bi_2O_3 and Sb_2O_3.

The correlation is preliminary in the sense that not all our samples are characterized as to their band gap and crystal structure, in cases where different polymorphs exist. The scatter in literature data and variation in band-gap between different crystalline polymorphs are represented in the figure as error bars, where appropriate[33]. Nonetheless the broad success of the correlation may readily be understood in terms of equation (3), our muonium data mimicking the case of hydrogen defect centres that are truly isolated or in the limit of extreme dilution. The relative stability of the atomic state and a complex of a proton or muon with one electron at the bottom of the conduction band is defined by the interplay of the energy gain from OH^- formation and the energy required to excite an electron from the atomic hydrogen or muonium level to the conduction-band minimum.

In order to quantify this interplay, we introduce three parameters that are in principle spectroscopically observable, namely the energy splittings labelled Δ_1, Δ_2 and Δ_3 in figure 1. The energy of an oxide with atomic hydrogen as a single interstitial centre (figure 1(a)) may then be written $E_0 + \Delta_1$, where E_0 is the internal energy of the pure undefective material at absolute zero. Similarly, the energy of the hydride ion is $E_0 + 2\Delta_2$. The energy of the interstitial proton is $E_0 - 2\Delta_3$ and that of a shallow-donor complex with a conduction-band electron (figure 1(b)) is $E_0 - 2\Delta_3 + E_g$. Note that not all these states are necessarily stable in a particular oxide. The energy difference between the deep atomic state (figure 1(a)) and the $[H^+ + e_c]$ shallow-donor complex (figure 1(b)) is $E_g - 2\Delta_3 - \Delta_1$, so that the condition for the absolute stability of H^0 is $2\Delta_3 + \Delta_1 < E_g$. This describes the energetics of reaction (3). Equivalently, the condition for the coexistence of isolated H^0 and a shallow complex $[H^+ + e_c]$,

[33] For CeO_2, the smaller of the two band-gaps proposed by Wuilloud *et al* (1984) is used as the relevant parameter, that is, the gap between the oxygen p-states and polaron like f-states of cerium. The larger gap corresponding to transitions onto d-states of cerium is reported to be 6 eV by these authors.

or for the crossover from one to the other, is

$$2\Delta_3 + \Delta_1 \approx E_g. \tag{22}$$

According to our data, oxides showing this metastability have the combination of parameters $2\Delta_3 + \Delta_1$ lying between 5 and 7 eV, describing how stabilization of H^+ and H^- are related. The correspondence with an alternative treatment of the ion insertion energies in terms of the interplay of Madelung and polarization energies (Cox 2003a, 2003b) is useful here. We make no claim for universality of this condition beyond the oxides, where it must relate to the unusual stability of the closed-shell hydroxide ion. Somewhat to our surprise, this criterion disregards structure and applies whatever the degree of disruption to anion–cation bonds: no correlation is found in table 2 between oxygen coordination and the occurrence of shallow states. It is true that the other examples of shallow states are found in materials with band-gaps between 0.8 and 3.5 eV, namely in InN, CdS, CdSe, CdTe and GaN, as well as in ZnO. However, normal muonium is seen in a variety of other materials with gaps below 5 eV, namely Si, Ge, GaAs, GaP, ZnS and ZnSe (as well as the elements As and I). For these, it is instead the significantly reduced muonium hyperfine constant which correlates with band-gap (see, e.g. Cox 2003a or Cox and Johnson 2005). Muonium exhibits metastability in Si, Ge, GaAs and GaP, and also in diamond, but both the cage-centred and bond-centred species have compact electronic orbitals. (The bond-centred states may be classed as deep polarons, in the spirit of figure 1(c), and evidently the three-Δ model could be readily extended to describe these.) Beyond the oxides, only in CdTe and GaN has a coexistence of shallow and atomic muonium been reported (Gil *et al* 2001a, Shimomura *et al* 2004).

Within the three-Δ model, the switching levels may also be obtained by recalling their definition as the value of the Fermi level, E_F, at which the free energies of the corresponding states are equal. Thus the condition for (+/0) switching is $E_0 - 2\Delta_3 + E_F = E_0 + \Delta_1$, so that the donor level, measured with respect to the valence-band maximum, is

$$E(+/0) = 2\Delta_3 + \Delta_1. \tag{23}$$

Similarly, the acceptor and pinning levels are, respectively,

$$E(0/-) = 2\Delta_2 - \Delta_1 \tag{24}$$

and

$$E(+/-) = \Delta_2 + \Delta_3. \tag{25}$$

The charge disproportionation energy U between two hydrogen atoms (equation (6)) can be obtained from the same considerations as $U = 2(\Delta_2 - \Delta_3 - \Delta_1)$, giving the condition for $U < 0$ as

$$\Delta_2 < \Delta_1 + \Delta_3. \tag{26}$$

Importantly, conditions (22) and (26) are not mutually exclusive, the one relating to isolated hydrogen atoms and the other to those in communication. The fact remains, however, that the implied importance of hydride ions in oxides has not been demonstrated experimentally.

7.6. Implications for doping

Ideally, the muonium studies would determine both the donor (0/+) and acceptor (−/0) levels in each material, allowing a full characterization in the manner of figure 2. Whereas the present work has identified donor levels both deep and shallow, identification of the deep acceptor levels remains uncertain. The positions of the pinning level and the values of U in each material remain indeterminate, therefore, and no firm predictions for hydrogen doping can be made.

Equations (23)–(26) relate all these levels and quantities to our Δ parameters, suggesting that they may be accessible by other forms of spectroscopy. In particular, equation (25) implies that the condition for hydrogen-induced electronic conductivity may alternatively be given as

$$\Delta_2 + \Delta_3 \geqslant E_g. \tag{27}$$

Tantalizingly, it appears to be exactly in those oxides under primary consideration for gate dielectrics where we find examples of coexisting deep and shallow muonium states. Given also the likely importance of out-of-equilibrium conditions in oxides, suffice it to say that the *possibility* of hydrogen-induced conduction should be borne in mind for all those oxides where shallow-donor muonium states are observed, and that the muonics techniques and analogies offer a convenient means of screening other materials for this behaviour.

Acknowledgments

We wish to record our thanks A M Stoneham, D Eshchenko, R L Lichti, E Roduner and A Weidinger, for invaluable discussions and correspondence. The data were recorded in successive allocations of muon beamtime at the CCLRC ISIS Facility between 2003 and 2005. JLG would like to acknowledge financial support from International Sematech; JMG and the Coimbra Group likewise acknowledge support by FCT/FEDER European Funds (grant POCTI/35334/FIS/2000—Portugal).

Appendix A. Interplay of shallow and deep states

A.1. Amplitude versus linewidth analysis

For several of the materials of figure 6 it proves possible to view the μSR spectrum as a superposition of broad and narrow lines, both centred on the muon Larmor frequency. In the time domain signals, this corresponds to components with fast and slow relaxation rates: the fitted amplitudes are shown in figure A.1. For WO_3 and rutile TiO_2 we take the amplitude of the fast-relaxing signal to be a direct measure of the yield of the shallow-donor state ($Mu^0_{shallow}$): it disappears in a temperature range appropriate to shallow-donor ionization, with a concomitant increase of the slow-relaxing signal, which we take to represent the ionic (Mu^+) state. The fitted lines in figure A.1 are simultaneous fits to the Mu^+ and Mu^0 fractions, using equations (16) and (17) together. The resulting activation energies are consistent with those of figure 6, corroborating the more simplistic linewidth analysis.

In WO_3, the fast relaxation rate is several inverse microseconds, suggesting unresolved or distributed hyperfine parameters of at least a few MHz. Consistent with this, a similar relaxation is visible in zero field but is suppressed or decoupled in low longitudinal fields of a few mT. For both WO_3 and TiO_2, these two components together account for the full incoming muon polarization, so that $Mu^0_{shallow}$ and Mu^+ are the only two states in play. This is not so in HfO_2. Here a proportion of the polarization is missing in our transverse-field precession signals but is recovered in substantially higher longitudinal fields of a few 100 mT in a manner which identifies it as normal muonium, i.e. Mu^0_{atomic}, as described in section 5. Evidently the deep and shallow states coexist at low temperature in HfO_2, since a signature of shallow-donor ionization is visible in figure A.1(c), although the atomic state persists to well above room temperature. Similarly it appears that Mu^0_{atomic} and $Mu^0_{shallow}$ coexist in ZrO_2 and YSZ but not in SnO_2.

Particularly illuminating is the case of YSZ: this exhibits three components in the Larmor precession signal, shown in figure A.1(d), whose relaxation rates we call slow, intermediate and fast. Together they account for the full incoming muon polarization. There is no promptly

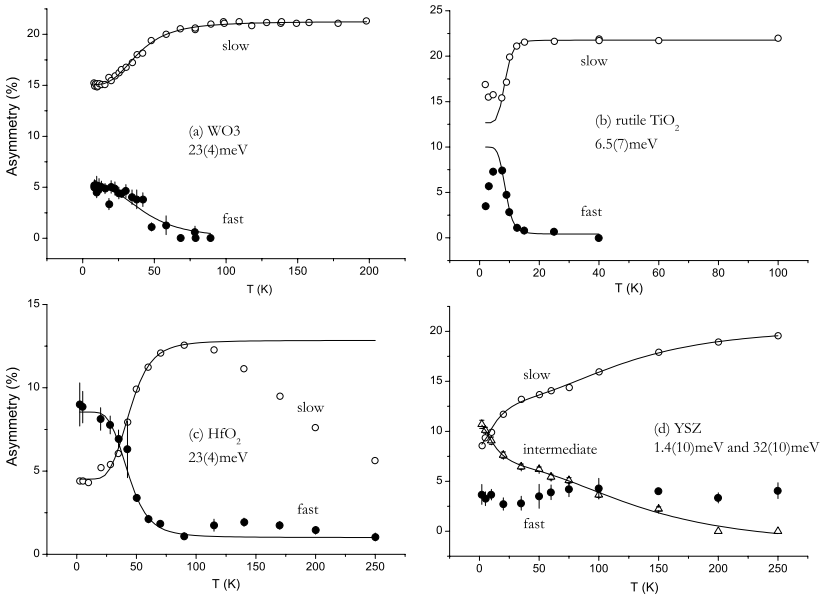

Figure A.1. Variation of the amplitudes with temperature, for components of the precession signals with distinct relaxation (damping) rates. (These are expressed as their contribution to the muon decay asymmetry: full polarization here corresponds to an asymmetry of 21–22%, according to instrument setup. Note the missing polarization in the HfO_2, recovered in longitudinal field.) The lines are model fits, as described in the text, yielding ionization energies as indicated.

formed atomic muonium in YSZ, therefore, although the fast relaxation of about 4 μs^{-1} may in this case be assigned to its delayed formation: this rate is approximately constant up to room temperature, as is the corresponding amplitude. The intermediate relaxation rate averages 0.3 μs^{-1} and is taken to represent the unresolved hyperfine splitting of $Mu^0_{shallow}$; the slow rate (which averages 0.02 μs^{-1} and is fixed to this value in the analysis) corresponds to a narrow spectral line which we assign to Mu^+. As the amplitude of the $Mu^0_{shallow}$ component is lost with increasing temperature, it is fully transferred to the Mu^+ signal, consistent either with ionization or with increasingly rapid spin dynamics. The fitted temperature dependences here suggest the involvement of two activation energies and we assign the larger value to the shallow-donor ionization. (This differs from the result of the simpler analysis of figure 6(e)—we enter both values in table 3.) The smaller value is too small for a Boltzmann or Arrhenius analysis to be strictly valid; we assign it to some form of spin relaxation—either spin–lattice relaxation within the isolated centres or—recalling similar behaviour in CdS and in samples of CdTe where the native defect concentration is manipulated by sample preparation (Corregidor *et al* 2004)—spin-exchange communication with other defects, e.g. via hopping transport.

A.2. CeO_2

Similarly, the separation of precession signals near the muon Larmor frequency in CeO_2 into components with fast and slow relaxation is shown in figure A.2(a). Their complementary variation above about 15 K shows the shallow-donor signature, with an effective ionization energy of 33 ± 7 meV. Below this temperature, however, their amplitudes sum to less than the full muon polarization and this missing fraction is fully recovered in longitudinal field only below 6 K (figure A.2(b)). Here the repolarization curve is fitted with a static hyperfine tensor

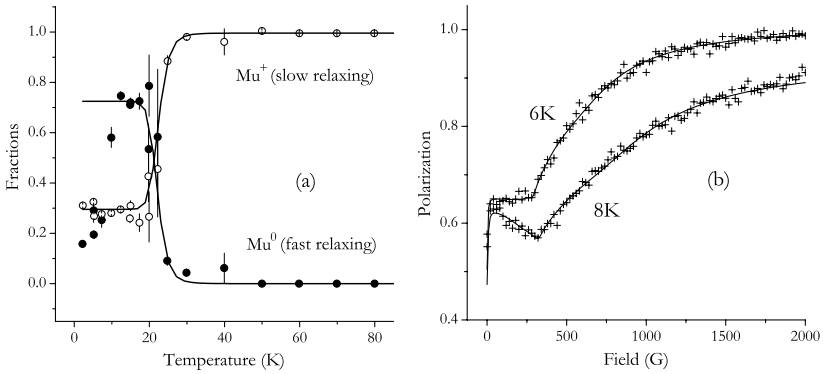

Figure A.2. μSR data for CeO_2 in (a) transverse field, showing the effective ionization of a shallow muonium state, and (b) longitudinal field, with static and dynamic repolarization curves fitted.

having a low contact term of $A_{\rm iso} = 0.8 \pm 0.2$ MHz and a relatively large dipolar term of 17 ± 4 MHz.[34] These parameters represent a spin density distribution that is too compact and asymmetric to be hydrogenic: it is probably of the polaronic type sketched in figure 1(c), the dipolar term indicating the centre of gravity of the distribution to be displaced 0.34 nm from the muon site. The partial repolarization at 8 K can be accounted for by the onset of dynamics, and is fitted here by including a spin-exchange rate of about 1 MHz (Lord 2006). It may well be that faster spin-exchange rates collapse the transverse-field spectrum to a single line above 15 K and are responsible for the subsequent narrowing at higher temperature. If this is so, the linewidth data imply spin-flip rates increasing to over 100 MHz above 40 K.

A.3. The sapphire puzzle

Sapphire deserves a mention here, as a material in which the delayed conversion of a diamagnetic state into atomic muonium has been extensively documented, beginning with the work of Minaichev *et al* (1970a, 1970b) and Kreitzman *et al* (1986). Unlike the oxides of figure 6, the damping rate of the Larmor precession signal in sapphire shows a thermally activated behaviour above 20 K and is taken to be a direct measure of the muonium formation rate. Various interpretations have been placed on this temperature dependence: Storchak *et al* (1997) relate it to electron capture by the positive ion, Brewer *et al* (2000) to conversion from the negative ion. In the latter case, the question of why the implanted muon picks up two electrons in the first place appears to be answered by the calculations of Peacock and Robertson (2003), who predict H^- to be the stable charge-state of hydrogen in Al_2O_3–sapphire. However, the activation energy for thermal conversion to the neutral state is remarkably low: Storchak *et al* (1997) report Arrhenius behaviour above 20 K with $E_{\rm a} = k_{\rm B} \times 130$ K $= 11$ meV. If this represents electron ionization, $Mu^- \rightarrow Mu^0 + e$, one must draw the doubly occupied level close to the conduction band, i.e. set $\Delta_2 = E_{\rm g} - 11$ meV in figure 1(a); by implication, the hydride ion acts as a shallow donor, which is unprecedented. Otherwise one must draw the level close to the valence band (small Δ_2) and invoke hole capture, $Mu^- + h \rightarrow Mu^0$. This question is clearly still unresolved.

Here it is noteworthy that H^- has also been predicted to be the stable charge-state of hydrogen in Y_2O_3 (Ragnarsson *et al* 2001), yet there is no indication that our data in figure 6(f)

[34] Note the cusp-like shape characteristic of anisotropic centres in polycrystalline samples, cf. figure 10. Note also that purely isotropic couplings are decoupled in fields of order $A_{\rm iso}/\gamma_\mu$, whereas dipolar terms (of similar magnitude) require much larger decoupling fields of order $D/\gamma_{\rm e}$.

refer to the negative, rather than the positive, muonium charge-state. It is for La_2O_3 that our linewidth data, above about 50 K, show some similarities with those for Al_2O_3.

Appendix B. Muonium formation in Bi_2O_3 and Sb_2O_3

Reports of unexpected magnetism in Bi_2O_3 and Sb_2O_3 stem chiefly from otherwise unexplained features in NQR spectra (see, for example, Kravchenko and Orlov 1994, Semin and Bogulavsky 1996, Kharkovskii *et al* 1996). μSR data has also been invoked in support of large internal fields in Bi_2O_3, by Duginov *et al* (1994b); in our view, however, the fast muon depolarization observed by these authors may be attributed simply to the formation of atomic muonium. The implanted muons thermalize as the Mu^+ ion and a proportion remain in this charge state; their Larmor precession frequency corresponds exactly to the externally applied field, so that there is no significant internal field at whatever site or sites are adopted by this fraction. The rest pick up electrons to form muonium and are depolarized by the muonium hyperfine field[35]. It does not appear necessary to invoke any anomalous moment on, or internal field from, the Group-V cations. In Bi_2O_3, the muon polarization is entirely recovered in longitudinal field as expected for atomic muonium, as shown in figure 8(a). We note also that, above room temperature, a diamagnetic fraction of unity is recovered gradually as the muonium fraction disappears towards 500 K (figure 9(a)), with no abrupt change that might be expected to accompany a magnetic transition.

The same is undoubtedly true of Sb_2O_3 although for this material the repolarization data are admittedly less decisive: unusually fast spin lattice relaxation obscures the normal muonium signature. There is no such missing fraction or fast depolarization in our data for Sb_2O_5.

References

Abragam A 1961 *Principles of Nuclear Magnetism* (Oxford: Oxford University Press)
Adler D and Yoffa E J 1976 *Phys. Rev. Lett.* **36** 1197
Amato A 1997 *Rev. Mod. Phys.* **69** 1119
Amato A, Degueldre C, Hoffelner W and Zimmermann U 2003 *PSI Scientific Report 2002* vol III, p 123 (ISSN 1423-7326)
Anderson P W 1975 *Phys. Rev. Lett.* **34** 953
Baker J M, Cox A, O'Connell A J and Ward R C C 1991 *J. Phys.: Condens. Matter* **3** 6189
Baumeler Hp *et al* 1986 *Hyperfine Interact.* **32** 659
Bech Nielsen B, Johannesen P, Stallinga P and Bonde Nielsen K 1997 *Phys. Rev. Lett.* **79** 1507
Beck R, Meier P F and Schenck A 1975 *Z. Phys.* B **22** 109
Berzelius J J 1815 *Afhandlingar i Fysik, Kemi och Mineralogie* **4** 293
Blöchl P 2000 *Phys. Rev.* B **62** 6158
Blundell S J *et al* 2003 *Physica* B **326** 527
Boekema C *et al* 1986 *Hyperfine Interact.* **32** 667
Boekema C, Ruegg K J, Kündig W and Hofmann W P 1981 *Hyperfine Interact.* **8** 609
Bonde Nielson K, Bech Nielsen B, Hansen J, Andersen E and Andersen J U 1999 *Phys. Rev.* B **60** 1716
Brewer J D *et al* 2000 *Physica* B **289/290** 428
Brewer J H 1981 *Hyperfine Interact.* **8** 375
Brewer J H 1983 *TRIUMF data dated 1978, shown at the Yamada Conference on Muon Spin Rotation and Associated Problems (Shimoda, 1983)* but otherwise unpublished
Brewer J H 2002 *TRIUMF data* private communication
Brewer J H, Crowe K M, Gygax F M, Johnson R F, Patterson B D, Fleming D G and Schenck A 1973 *Phys. Rev. Lett.* **31** 143

[35] The depolarization rate is either a direct measure of the muonium formation rate or is some superposition of the allowed muonium spin-state transition frequencies, whichever is the slower. The reported rates of between 5 and 30 μs^{-1} imply delayed muonium formation, although the temperature dependence is opposite to that in sapphire!

Brewer J H, Crowe K M, Gygax F N and Schneck A 1975 *Muon Physics* vol 3, ed V W Hughes and C S Wu (New York: Academic) p 3
Butler M A and Ginley D S 1978 *J. Electrochem. Soc.* **39** 275
Catlow C R A, Baram P S, Parker S C, Purton J and Wright K V 1995 *Phil. Trans. R. Soc.* A **350** 265
Chester P F 1961 *J. Appl. Phys.* **10** 2233
Chester P F 2004 *Hydrogen in Oxides Workshop (Royal Institution of Great Britain, London, 21 April 2004)* private communication
Corregidor V, Martin Y, Marero D, Gil J M and Dieguez E 2004 *Europhys. Lett.* **67** 247
Cox S F J 1987 *J. Phys. C: Solid State Phys.* **20** 3187
Cox S F J 2003a *J. Phys.: Condens. Matter* **15** R1727
Cox S F J 2003b *Physica* B **340–342** 250
Cox S F J and Hartmann O 2006 to be published
Cox S F J and Johnson C 2005 *Proc. XIII-HFI (Bonn, Aug. 2004)*; *Hyperfine Interact.* plus references therein
Cox S F J, Cottrell S P, Hopkins G A, Kay M and Pratt F L 1997 *Hyperfine Interact.* **106** 85 (doi:10.1007/510751-005-9041-3)
Cox S F J, Cottrell S P, Lord J S, Vilão R C, Alberto H V, Piroto Duarte J P, Gil J M, Ayres de Campos N, Davis E A, Charlton M, Van der Werf D P, Keeble D J, Lichti R L and Weidinger A 2005 *Proc. 27th Int. Conf on the Physics of Semiconductors (Flagstaff Arizona, July 2004)*; *AIP Conf. Proc.* **772** 193
Cox S F J, Lord J S, Cottrell S P, Gil J M, Alberto H V, Keren A, Prabhakaran D, Scheuermann R and Stoykov A 2006 *J. Phys.: Condens. Matter* **18** (Accompanying paper 'Oxide Muonics I')
Cox S F J *et al* 2001a *Phys. Rev. Lett.* **86** 2601
Cox S F J *et al* 2001b *J. Phys.: Condens. Matter* **13** 9000
Cox S F J and Symons M C R 1986 *Chem. Phys. Lett.* **126** 516
Dalmas de Réotier P and Yaouanc A 1997 *J. Phys.: Condens. Matter* **9** 9113
Davis E A 2004 Zinc oxide as a material for micro- and optoelectronic applications *NATO Advanced Research Workshop (St Petersburg, June 2004)*
Davis E A, Cox S F J, Lichti R L and Van de Walle C G 2003 *Appl. Phys. Lett.* **82** 592
Dawson W K, Nishiyama K, Macrae R and Nagamine K 1997 *Hyperfine Interact.* **106** 97
Donnelly P A, Charlton M, Van der Werf D P, Cottrell S P and Cox S F J 2006 to be published
Duginov V N *et al* 1994a *Hyperfine Interact.* **85** 317
Duginov V N *et al* 1994b *Hyperfine Interact.* **85** 197
Gavartin J L 2005 unpublished
Gavartin J L, Shluger A L, Foster A S and Bersuker G I 2005 *J. Appl. Phys.* **97** 053704
Gil J M *et al* 2001a *Phys. Rev.* B **64** 075205
Gil J M *et al* 2001b *J. Phys.: Condens. Matter* **13** L613
Goss J 2003 *J. Phys.: Condens. Matter* **15** R551
Gross B, Dilger H, Scheuermann R, Päch M and Roduner E 2001 *J. Phys. Chem.* A **105** 10012
Harris S W 1991 *Thesis* University of Uppsala (ISBN 91-554-2794-4)
Harshman D R 1986 *Hyperfine Interact.* **32** 847
Hartmann O, Harris S S, Wäppling R and Hempelmann R 1992 *Phys. Scr.* **45** 402
Hjelm A, Granqvist C G and Wills J M 1996 *Phys. Rev.* B **54** 2436
Hofmann D M *et al* 2002 *Phys. Rev. Lett.* **88** 045504
Houssa M 2004 *High-κ Gate Dielectrics* ed M Houssa (Bristol: Institute of Physics Publishing) p 467
Isoya J, Weil J A and Halliburton L E 1981 *J. Chem. Phys.* **74** 5436
Ivanter I G and Smilga V P 1968 *Zh. Eksp. Teor. Fiz.* **55** 1521
Ivanter I G and Smilga V P 1969 *Sov. Phys.—JETP* **28** 796 (Engl. Transl.)
Kang J, Lee E-C and Jin Y-G 2004 *Appl. Phys. Lett.* **84** 3894
Keeble D J 2006 to be published
Kharkovskii A I, Nizhankovskii V I, Kravchenko E A and Orlov V G 1996 *Z. Naturf.* a **51** 665
Kiefl R F *et al* 1982 *Phys. Rev.* B **26** 2432
Kiefl R F *et al* 1986 *Phys. Rev.* B **34** 1474
Kılıç Ç and Zunger A 2002 *Appl. Phys. Lett.* **81** 73
Kravchenko E A and Orlov V G 1994 *Z. Naturf.* a **49** 418
Kreitzman S R, Kiefl R F, Noakes D R, Brewer J H and Ansaldo E J 1986 *Hyperfine Interact.* **32** 521
Kudo H and Okuno K 1986 *J. Nucl. Mater.* **138** 31
Lichti R L 1995 *Phil. Trans. R. Soc.* A **350** 323
Lord J S 2006 Computer simulation of muon spin evolution *Proc. μSR 2005 (Oxford, Aug. 2005)*; *Physica* B at press

Lord J S, Cottrell S P and Williams W G 1998 *J. Phys.: Condens. Matter* **10** 7975
Lord J S, Cox S F J, Alberto H V, Piroto Duarte J and Vilão R C 2004 *J. Phys.: Condens. Matter* **16** S4707
Madelung O (ed) 1996 *Semiconductors—Basic Data* (Berlin: Springer)
See also Madelung O 1992 *Data in Science and Technology, Semiconductors other than the Group IV and III–V Compounds* (Berlin: Springer)
Memming M 1983 *Comprehensive Treatise on Electrochemistry* vol 7 (New York: Plenum) p 543
Minaichev E V, Mysaischeva G G, Obhukhov Yu V, Roganov V S, Saval'ev G I and Firsov V G 1970a *Zh. Eksp. Teor. Fiz.* **58** 1586
Minaichev E V, Mysaischeva G G, Obhukhov Yu V, Roganov V S, Saval'ev G I and Firsov V G 1970b *Sov. Phys.—JETP* **31** 849 (Engl. Transl.)
Myasischeva G G, Obukhov Yu V, Roganov H S and Firsov V G 1967 *Zh. Eksp. Teor. Fiz.* **53** 451
Myasischeva G G, Obukhov Yu V, Roganov H S and Firsov V G 1968 *Sov. Phys.—JETP* **26** 298 (Engl. Transl.)
Neugebauer J and Van de Walle C G 1995 *Phys. Rev. Lett.* **75** 4452
Norby T, Widerøe M, Glöcker R and Larring Y 2004 *Dalton Trans.* 3012
Ong C J 1983 *J. Phys. C: Solid State Phys.* **16** 4081
Osaka T and Shindo I 1984 *Solid State Commun.* **51** 421
Pantelides S T 1986 *Deep Centres in Semiconductors* (New York: Gordon and Breach) p 55
Patterson B D 1988 *Rev. Mod. Phys.* **60** 69
Peacock P W and Robertson J 2003 *Appl. Phys. Lett.* **83** 2025
Percival P W *et al* 1985 *Chem. Phys.* **95** 321
Perlson B D and Weil J A 1974 *J. Magn. Reson.* **15** 594
Poeppelmeier K 2002 *Science* **295** 1849
Poulsen F W 2001 *Solid State Ion.* **145** 387
Pratt F L 1997 *Phil. Mag. Lett.* **75** 371
Ragnarsson L A *et al* 2001 *Appl. Phys. Lett.* **78** 4169
Rignese G-M 2005 *J. Phys.: Condens. Matter* **17** R357
Robertson J 2000 *J. Vac. Sci. Technol.* B **18** 1785
Robertson J 2004 *Presentation to the Hydrogen in Oxides Workshop (The Royal Institution of Great Britain, London, April 2004)* unpublished, and private communications
Roduner E, Percival P W, Han P and Bartels D M 1995 *J. Chem. Phys.* **102** 5989
Ruegg K J, Boekema C, Kündig W, Meier P F and Patterson B D 1981 *Hyperfine Interact.* **8** 547
Schefzik M *et al* 1998 *Solid State Commun.* **107** 395
Schefzik M *et al* 2000 *Physica* B **289–290** 511
Schenck A 1985 *Muon Spin Rotation Spectroscopy* (Bristol: Hilger) plus references therein
Schmickler W and Schultze J W 1986 *Modern Aspects of Electrochemistry* vol 17 (New York: Plenum) p 357
Scholz G and Stösser R 2002 *Phys. Chem. Chem. Phys.* **4** 5448
Semin G K and Bogulavsky A A 1996 *Chem. Phys. Lett.* **251** 250
Senba M 2005 *J. Phys. B: At. Mol. Opt. Phys.* **38** 1305
Shah R, De Vita A and Payne M C 1995 *J. Phys.: Condens. Matter* **7** 6981
Shimomura K, Kadono R, Oshishi K, Mizuta M, Saito M, Chow K H, Hitti B and Lichti R L 2004 *Phys. Rev. Lett.* **92** 135505
Shimomura K, Nishiyama K and Kadono R 2002 *Phys. Rev. Lett.* **89** 255505
Shluger A L, Foster A S, Gavartin J L and Sushko P V 2003 *Defects in Widegap Oxides* ed J Greer, A Korkin and J Labanowski (Amsterdam: Elsevier) p 157
Shluger A L, Itoh N and Koda K 1991 *J. Phys.: Condens. Matter* **3** 9895
Spaeth J-M 1986 *Hyperfine Interact.* **32** 641
Spencer D P, Fleming D G and Brewer J H 1984 *Hyperfine Interact.* **17–19** 567
Steinsvik S, Larring Y and Norby T 2001 *Solid State Ion.* **143** 103
Stesmans A and Afanas'ev V V 2004 *High-κ Gate Dielectrics* ed M Houssa (Bristol: Institute of Physics Publishing) p 217
Stoneham A M 1975 *Theory of Defects in Solids* (Oxford: Clarendon) reprinted as an Oxford Classic, 2001
Stoneham A M and Dhote J 1997 *Crystal Data* see www.oxmat.co.uk/Crysdata plus references therein
Stoneham A M, Shluger A L and Gavartin J L 2005 *J. Phys.: Condens. Matter* **17** S2027
Storchak V G, Brewer J H and Morris G D 1997 *Phys. Rev.* B **56** 55
Storchak V G, Eschenko D G and Brewer J H 2004 *J. Phys.: Condens. Matter* **16** S4761
Suryanarayana D and Weil J A 1976 *J. Chem. Phys.* **64** 510
Tanigawa H and Tanaka S 2002 *J. Nucl. Mater.* **307–11** 1446
Tanigawa H, Tanaka S, Enoeda M and Akiba M 2004 *J. Nucl. Mater.* **329–33** 1291

Tyryshkin A M, Lyon S A, Astashkin A V and Raitsimring A M 2003 *Phys. Rev.* B **68** 193207
Van de Walle C G 2000 *Phys. Rev. Lett.* **85** 1012
Van de Walle C G, Denteneer P J H, Bar-Yam Y and Pantelides S T 1989 *Phys. Rev.* B **39** 10791
Van de Walle C G and Neugebauer J 2003 *Nature* **423** 626
Venkatesan M, Fitzgerald C B and Coey J M D 2004 *Nature* **430** 630
Walstedt R E and Walker L R 1974 *Phys. Rev.* B **9** 4857
Weeks R A and Abraham M 1965 *J. Chem. Phys.* **42** 68
Weil J A 1981 *Hyperfine Interact.* **8** 317
Wuilloud E, Delley B, Schneider W-D and Baer Y 1984 *Phys. Rev. Lett.* **53** 202
Yokozawa A and Miyamoto Y 1997 *Phys. Rev.* B **55** 13783